DEVELOPMENT OF PLA-BASED COMPOSITES EMPLOYING CELLULOSE NANOCRYSTALS EXTRACTED FROM RICE BRAN WASTE

BY

WITITA LAOSAMATHIKUL

A THESIS SUBMITTED IN PARTIAL FULFILLMENT OF
THE REQUIREMENTS FOR THE DEGREE OF MASTER OF
ENGINEERING (ENGINEERING TECHNOLOGY)
SIRINDHORN INTERNATIONAL INSTITUTE OF TECHNOLOGY
THAMMASAT UNIVERSITY
ACADEMIC YEAR 2015

DEVELOPMENT OF PLA-BASED COMPOSITES EMPLOYING CELLULOSE NANOCRYSTALS EXTRACTED FROM RICE BRAN WASTE

BY

WITITA LAOSAMATHIKUL

A THESIS SUBMITTED IN PARTIAL FULFILLMENT OF
THE REQUIREMENTS FOR THE DEGREE OF MASTER OF
ENGINEERING (ENGINEERING TECHNOLOGY)
SIRINDHORN INTERNATIONAL INSTITUTE OF TECHNOLOGY
THAMMASAT UNIVERSITY
ACADEMIC YEAR 2015

DEVELOPMENT OF PLA-BASED COMPOSITES EMPLOYING CELLULOSE NANOCRYSTALS EXTRACTED FROM RICE BRAN WASTE

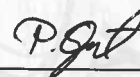A Thesis Presented

By

WITITA LAOSAMATHIKUL

Submitted to
Sirindhorn International Institute of Technology
Thammasat University
In partial fulfillment of the requirements for the degree of
MASTER OF ENGINEERING (ENGINEERING TECHNOLOGY)

Approved as to style and content by

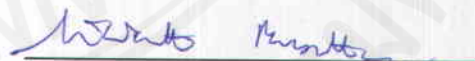Advisor and Chairperson of Thesis Committee   _____

(Assoc. Prof. Dr. Pakorn Opaprakasit)

Co-Advisor   _____

(Dr. Kittiwut Kasemwong)

Committee Member and
Chairperson of Examination Committee   _____

(Asst. Prof. Dr. Siwarutt Boonyarattanakalin)

Committee Member   _____

(Prof. Dr. Takeshi Serizawa)

December 2015

i

Abstract

DEVELOPMENT OF PLA-BASED COMPOSITES EMPLOYING CELLULOSE
NANOCRYSTALS EXTRACTED FROM RICE BRAN WASTE

by

WITITA LAOSAMATHIKUL

Bachelor of Engineering: Thammasat University, 2013

Rice bran waste (RBW) is a bio-residue from rice bran oil extraction process, which is generated in large amount every year. In this work, rice bran waste is used as raw materials in the preparation of cellulose nanocrystals (CNC). The raw material is extracted by alkali extraction and bleaching treatment to produce rice bran cellulose (RBC) by removed hemicellulose and lignin. Subsequently, the crystalline domains are extracted from this cellulose to form CNC by acid hydrolysis. Structures and properties of the resulting CNC are characterized. The results suggest that the uniform-sized CNC is in the form of high-purity single crystal, which exhibits good thermal properties and can be highly dispersed when used in the preparation of nanocomposite materials. CNC is mixed with poly(lactic acid) or PLA to generate biodegradable films with 0.2 and 0.5 wt%. Moreover, poly(vinyl alcohol) or PVA is used as a surfactant to improve the dispersion between CNC and PLA. As the results, CNC/PLA composite films have better mechanical properties, especially with 0.2wt% with PVA surfactant. The tensile strength and Young's modulus increase about 7% and 12%, respectively, compare to neat PLA. The higher crystallinity of CNC also affects to improve thermal properties and water vapour barrier properties.

Keywords: cellulose nanocrystals, composites, poly(lactic acid)

Acknowledgements

Table of Contents

List of Figures

List of Tables

Chapter 1
Introduction

Most commercial plastics are not biodegradable since their structures are not naturally occurred, and they are typically composed of artificial synthetic polymers (Kržan, 2012). In contrast, biodegradable plastics such as poly(lactic acid) or PLA, which are derived from renewable resources such as starch, are attractive in many applications. This is because PLA is biodegradable thermoplastic polyester (Haafiz et al., 2014). Due to its biodegradable properties and easy in processing, PLA are commercially used in many applications, including biomedical products, food packaging, and automotive materials. PLA is considered a good alternative to petroleum-based polymers. However, the material has relatively poor mechanical properties, in comparison with fossil-based commercial plastics (Lee et al., 2013). Many researchers concentrate on improvements of physicochemical and mechanical properties of PLA by using various reinforcing materials that are environmental friendly, i.e. can be obtained from renewable sources or biomass (Pasquini et al., 2010).

Cellulose is one of the most interesting materials for use in reinforced biocomposites, because of its renewability, outstanding mechanical properties, low density, and biodegradability. Nanosized cellulose is considered an attractive reinforcing agent because of its good mechanical properties such as high tensile strength, high flexural strength, and high stiffness with low density (Haafiz et al., 2014; Lee et al., 2013). Cellulose nanocrystals (CNC) are generated by acid hydrolysis to dissolve amorphous fractions off, leading to high percentage of crystalline domains (Hebeish et al., 2014). Cellulose can be produced from various types of plants, and even waste such as biomass and agricultural residues (Maheswari et al., 2012; Rosa et al., 2010; Wanrosli et al., 2011).

Rice bran oil is oil product extracted from hard outer brown layers of rice after chaff (rice husk). This is very popular cooking oil in many countries, since it provides many health benefits such as cholesterol busting power, cancer protection, immunity boost or antioxidant etc.(Jhawer & Vakil). However, there are some residues from

rice bran oil process, which contains high amount of cellulose. This can be extracted and used in many applications. The aim of this research is to develop a process to produce cellulose nanowhiskers from rice bran waste. Cellulose in raw materials is hydrolyzed by acid hydrolysis to form cellulose nanocrystals. The materials are then used in properties enhancements of degradable PLA. This study focuses effects of CNC within PLA matrix on the composite's properties. The concentrations of CNC, which is isolated from rice bran, on the improvements in mechanical properties of PLA matrix, such as tensile strength, Young's modulus, and elongation at break are investigated. In addition, crystallization, morphological, physicochemical, and barrier properties are also examined.

In this study, rice bran waste from rice bran oil production process is used as a raw material for CNC preparation. The overview of this research consists of 4 main steps, which is the preparation of cellulose from rice bran waste, the preparation of cellulose nanocrystals, the preparation of PLA/CNC composite films, and characterizations of the reinforcing materials and composite films.

Chapter 2
Literature Review

Nowadays, environmental problems continue to increase every year. A major problem is due to overpopulation that cause the over consumption of resources. Synthetics materials such as plastics can cause pollution and waste dispersal problems. Therefore, these problems have to be reduced by using environmental friendly materials such as bio-based materials. Bio-based materials have been developed for many years, and cellulose is largely used as raw materials. It can be found in all plants, such as rice or rice bran waste.

2.1 Rice

Rice is the most popular food of the world, especially in many Asian countries. In Thailand, rice is a major food, and it is also one of economical products of Thailand. Rice can be separated into many types, depending on the amount of amylase and amylopectin in starch, which is the main part of rice. In addition, rice can be used in food processing for producing several new products such as alcohol beverage, noodle, rice flour, or even rice bran oil.

Figure 1 Structures of rice grains (http://www.foodietaste.com/)

Rice is one type of cereal grain that composes of many layers of hull. The outermost is rice husk, which contains cellulose and hemicelluloses. A rice grain contains germ and endosperm that is covered by rice bran, which has high protein and oil content, also with cellulose and hemicellulose(Pornchalermpong & Rattanapanon).

2.2 Rice bran oil extraction process
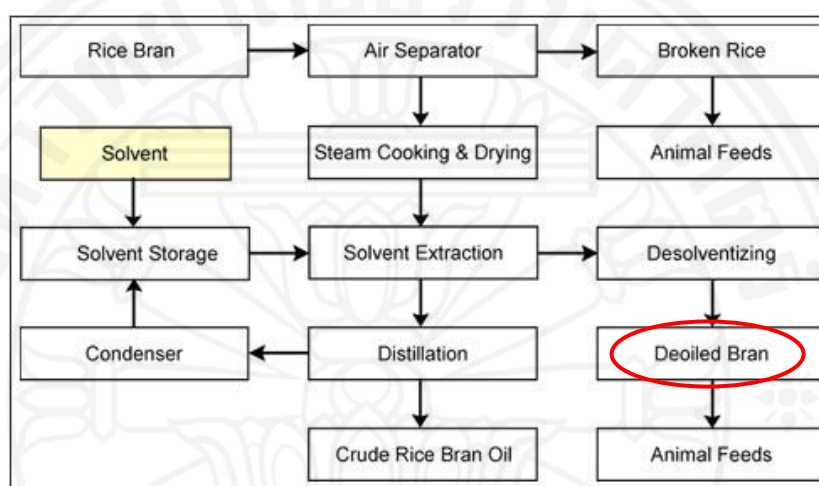
Figure 2 Overview of rice bran oil extraction process (http://www.thaiedibleoil.com/)

Rice bran is proven as one of effective oil resources, as it contains about 17% oil content, by weight. The rice bran oil extraction process is started by using raw material of rice bran. First, rice bran is screened to separate broken rice out by using an air separator. From this process, it generates broken rice as solid waste and dust in air. The broken rice is used as animal feeds. Subsequently, rice bran is passed to the steam cooking and drying unit, because it contains the moisture content of about 14-26% and to stop Lipase hydrolysis at the temperatures higher than 100 °C. The dust in air is generated as waste from this unit. After drying, rice bran is extracted by oilseed extraction solvents such as hexanes, the methylpentanes, and trichloroethylene. The solvent extracts oil out from rice bran. The oil is sent to a distillation unit and the residue is sent to a desolventizing unit. The oil extracted from the solvent extraction unit has to be distillated to separate the remaining solvent and get crude rice bran oil at the temperatures ranging from 230-240°C. The desolventizing unit is used to separate solvent out of rice bran. From this process, the solid residue of the deoiled

4

bran or rice bran after extraction is generated. This is used as a raw material in this research (Esler et al., 1952).

2.3 Rice bran

Many industrial processes and research work has widely used rice bran as a raw material, due to many benefits, such as high amounts of functional proteins and fats along with antioxidants, vitamins and trace minerals. Furthermore, it provides a concentrated source of fibers (McKEE & LATNER, 2000). Rice bran waste or deoiled bran from rice bran oil extraction process is brown color powder. This also contains high carbohydrate and dietary fiber contents with the percentage of 69.32% and 27.14%, respectively (see Appendix A).

2.4 Dietary fiber

Dietary fiber is considered as fibers that cannot be digested by human enzymes. Types of dietary fiber may be categorized according to their sources, solubility, fermentability and physiological effects. Dietary fiber mainly composes of cellulose, hemicellulose, lignin, pectin and other non-carbohydrate components (e.g., polyphenols, waxes, saponins, cutin, phytates, etc.) (Elleuch et al., 2011; Mudgil & Barak, 2013). Lignocellulose contains three components of cellulose, hemicellulose, and lignin, in which cellulose has larger amount of crystal than others. Accordingly the material is of interest in this study.
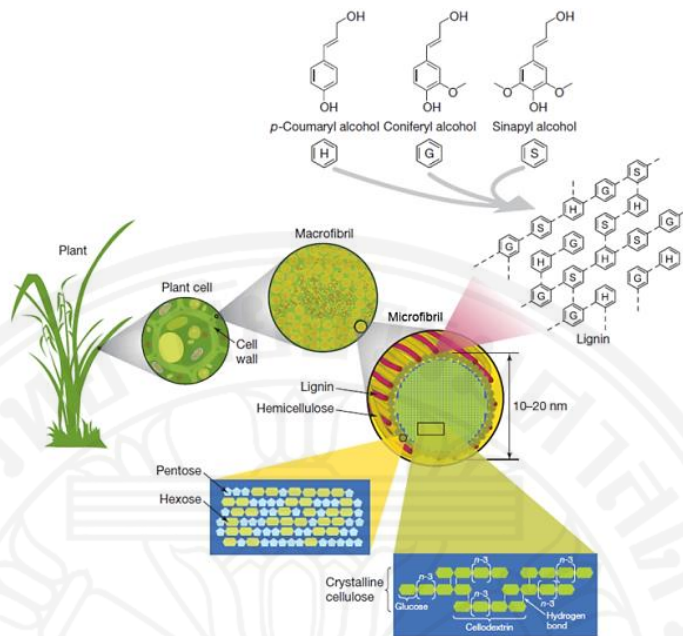
Figure 3 Structures of plant cell (Moran-Mirabal, 2013)

2.4.1 Cellulose

Cellulose is the most abundant polysaccharide found in nature and it forms the basic material of all plant fibers. It is an organic compound with the formula $(C_6H_{10}O_5)_n$, consisting of linear chains of several hundred to many thousands of $\beta(1{\rightarrow}4)$ linked D-glucose units. The degree of polymerization of the native cellulose depends on the source, which can be as high as 14,000 g/mol. Cellulose is one type of dietary fibers that has the structure of linear molecules packed tightly into long fibers. It is highly insoluble and resistant to digestion by human enzymes. Moreover, it is a significant structural component of primary cell wall of green plants and many forms of algae to provide structures and strength for cell wall. The molecules of cellulose have similar orientation to form microfibrils because of the frequent intermolecular hydrogen bonds within the cellulose matrix. Cellulose is composed of highly ordered crystalline structure and randomly distributed amorphous phase, depending on types of plants and the degree of organization of its structure. Cellulose can be also derived from some species of bacteria to form biofilms. The mechanical properties of each cellulose types are varied, depending on

6

cell geometry and geometrical conditions. Cellulose is resistant to strong alkali and oxidizing agents, but easily hydrolyzed by acids (Collard & Blin, 2014; Kalia et al., 2011; Mudgil & Barak, 2013).
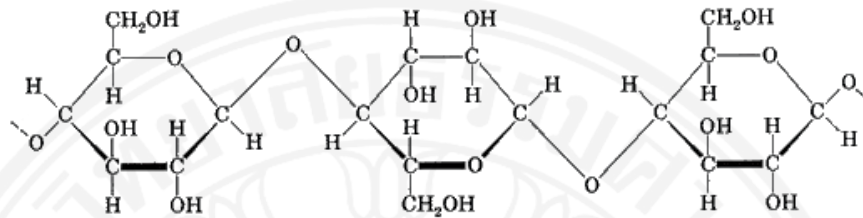
Figure 4 A cellulose structure
(http://antoine.frostburg.edu/chem/senese/101/consumer/faq/what-is-cellulose.shtml)

2.4.2 Hemicellulose

Hemicellulose differs from cellulose, since it composes of heterogeneous polysaccharide, which acts like a binder in plant cell wall. It contains smaller molecules of different sugar units, and contains both linear and branched molecules with 50–200 pentose units (xylose and arabinose) and hexose units (glucose, galactose, mannose, rhamnose, glucuronic and galacturonic acids). About one third of the dietary fiber in vegetables, fruits, legumes and nuts contains hemicellulose. Compared to cellulose, hemicellulose has chain branching structure while cellulose is mainly linear polymers. The degree of polymerization of the chains of hemicelluloses is also generally lower than 200. As a result, hemicelluloses are only constituted from amorphous phase (Collard & Blin, 2014; Kalia et al., 2011; Mudgil & Barak, 2013).

2.4.3 Lignin

The second most abundant biopolymers in the world is lignin, which can be commonly found in cell wall of woody tree species. It contents in woods ranges from 20% to 30% on a dry basis. Lignin includes aliphatic and aromatic constituents and exhibits as complex hydrocarbon polymers. In most pulp mills, it is considered a byproduct of the chemical pulping processes

(Kong et al., 2015). Lignin has variable compositions dependent on the plant source with highly branched and amorphous biomacromolecules. Due to its heterogeneity, lignin is unique by its lack of defined primary structure and aromatic functionality. It composes of three basic phenylpropane monomers as repeating units which are polymerized to "monolignols" to be p-coumaryl alcohol, coniferyl alcohol and sinapyl alcohol. Different types of plants contain different proportions of monomers because of several possible inter-connecting patterns between individual units that create an additional complexity to final molecule. Lignin is soluble in hot alkali solution but resistant to acid hydrolysis (Kalia et al., 2011; Norgren & Edlund, 2014).
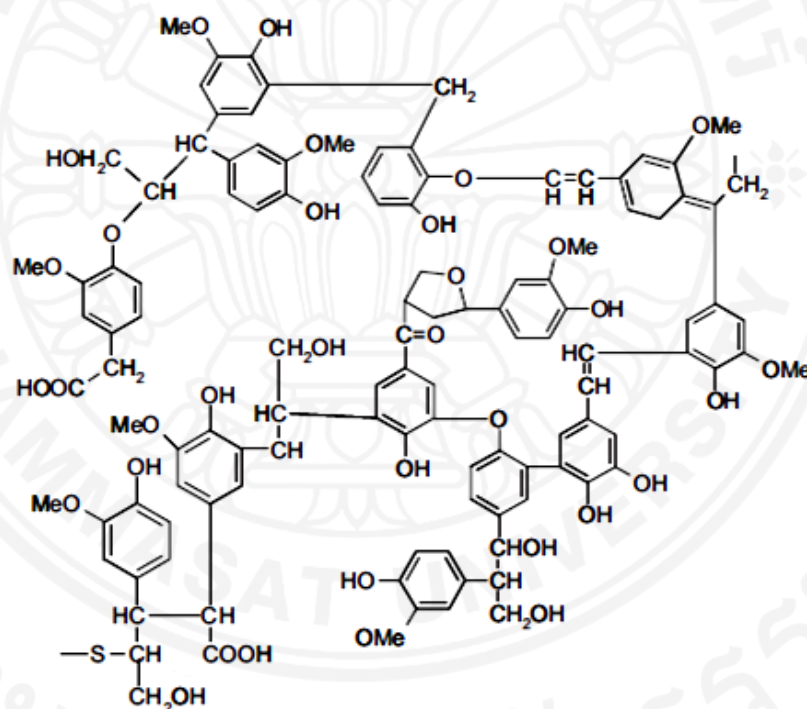
Figure 5 A structural model of a technical lignin fragment (kraft lignin) showing examples of important intra-molecular linkages (Norgren & Edlund, 2014)

2.5 Cellulose extraction

Since environmental problems are much more concerned, nowadays there is a number of research that study about the cellulose preparation and characterization

from biomass or natural residues. The methods to obtain cellulose can be divided into two processes, which are chemical treatment and bacteria extraction.

2.5.1 Cellulose extraction from bacteria

Baterial cellulose is cellulose produced from bacteria such as Acetobacter xylinus and Acetobacter hansenii. Inside the bacterial body, there is glucose chains produced and extrude out through tiny pores present on their cell envelope. The microfibrils are then formed by the combination of glucose chains to form cellulose ribbons or nanofibers.

Although bacterial cellulose has shown high potential as effective process for preparation with higher yield than from plant cellulose with higher crystallinity and mechanical strength, it has no antimicrobial and antioxidant properties to prevent infections. Therefore, it is not suitable for mass production in industries (Shah et al., 2013).

2.5.2 Cellulose extraction from chemical treatments

There are two main steps for chemical treatment process, which are alkali treatment and bleaching treatment. For alkali treatment, sodium hydroxide (NaOH) is used to mainly remove hemicellulose. For bleaching treatment, sodium chlorite ($NaClO_2$) is used to remove lignin and the remaining hemicellulose (Johar et al., 2012). The chemical concentration, ratio over liquor, extraction time and temperature are varied depending on types of the raw materials.
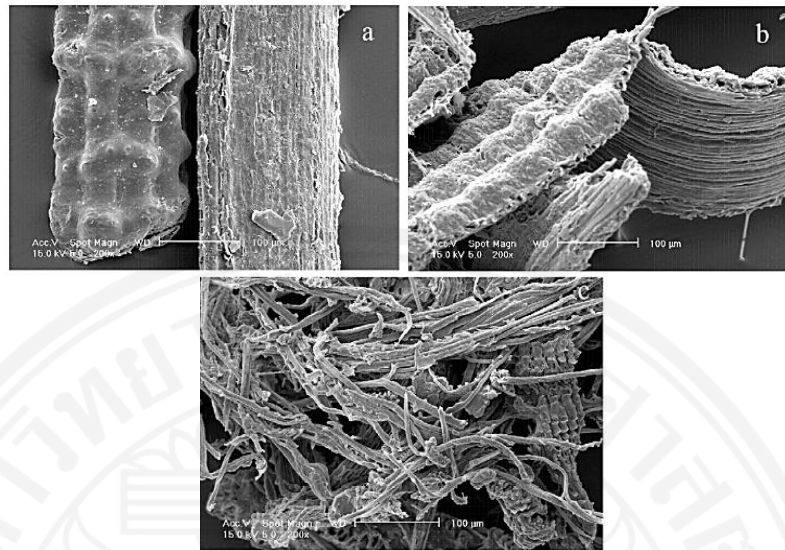
Figure 6 Scanning electron micrographs of (a) untreated rice husk fibres, (b) alkali-treated rice husk fibres, and (c) bleached rice husk fibres (Johar et al., 2012).

Maheswari, C. U., et al. studied the extraction and characterization of cellulose microfibrils from agricultural residues from coconut palm leaf sheath using 175 g/l sodium hydroxide (NaOH) solution for alkaline extraction process and 7 kg/m^3 sodium chlorite solution (NaClO$_2$) adjusted to a pH 4-4.2 by the addition of acetic acid-sodium acetate buffer, at 100 °C for 2 h using a fiber to liquor ratio of 1:50. It is shown that the resulting cellulose microfibrils had higher α-cellulose mass fraction from chemical characterization and crystallinity index from X-ray diffraction. The diameters of cellulosic fibers were in the range of 10-15 μm., from scanning electron microscopy results. Fourier transform infrared and Nuclear magnetic resonance spectroscopy showed that most of the hemicellulose and lignin in the leaf sheath fibers were removed after chemical treatments. Thermogravimetric analysis also showed that these cellulose microfibrils also had better thermal stability. Therefore, this indicated that their higher crystallinity in cellulose microfibrils can improve the thermal stability (Maheswari et al., 2012).

2.6 Cellulose nanocrystals (CNC)

Cellulose contains some amounts of amorphous regions, which decrease the strength in its structures. Hence, many research has attempted to remove these amorphous regions, to left only crystalline domains. This is called nanosized cellulose, such as cellulose nanocrystals, cellulose nanofibrils, or cellulose nanowhiskers. Johar, N, et al. prepared cellulose nanocrystals from rice husk by extracting cellulose fibers from rice husk using a similar methods to those described by Maheswari, C. U., et al. However, they used 4 wt% NaOH with reflux condition for alkaline treatment, and 1.7 wt% of aqueous chlorite for bleaching treatment. Sulfuric acid (H_2SO_4) was used to hydrolyzed amorphous regions in the cellulose and left only crystalline domains and formed nanocrystals. The material obtained after each stage of the treatments was carefully characterized and its chemical compositions were determined. The morphological structures of products from each step of treatments were different from one another and the diameters were reduced from 25–125 μm to 10–15 μm by using scanning electron microscopy (SEM) and transmission electron microscopy (TEM). Fourier transform infrared (FTIR) spectroscopy was used to confirm the removal of non-cellulosic constituents. From X-ray diffraction (XRD) analysis, the crystallinity increased after each step of chemical treatments. Thermal stability determined from thermogravimetric analysis (TGA) of cellulose nanocrystals was better than untreated rice husk fibres and rice husk cellulose (Johar et al., 2012).

Table 1 Summary on index of rice husks fibers at different stages of treatment (Johar et al., 2012)

Crystallinity index (CrI) of rice husks fibres at different stages of treatment.

Sample	CrI (%)
Untreated rice husk	46.8
Alkali treated rice husk	50.2
Bleached rice husk	56.5
Cellulose nanocrystals	59.0

Cellulose nanocrystals derived from other agro-industrial residues, such as soy hull, also showed similar results, which were size reduction, higher crystallinity, and higher thermal stability for potential use as reinforcing agents in nanocomposite preparations (Neto et al., 2013). Alemdar, A. & Sainwere, M. obtained nanofibers from wheat straw, whose diameters were determined in the range of 10–80 nm and lengths of a few thousand nanometers. When alkali and acid treatments were applied to wheat straw, the cellulose contents also increased from 43% to 84%, which was observed by chemical characterization (Alemdar & Sain, 2008). Furthermore, similar results were also observed in rubberwood (Hevea brasiliensis) (Jonoobi et al., 2011), empty fruit bunches (EFB) of oil palm (Elaeis guineensis) (Jonoobi et al., 2011), corncob (Silvério et al., 2013), coconut husk (Rosa et al., 2010), and sweet potato residue (H. Lu et al., 2013).
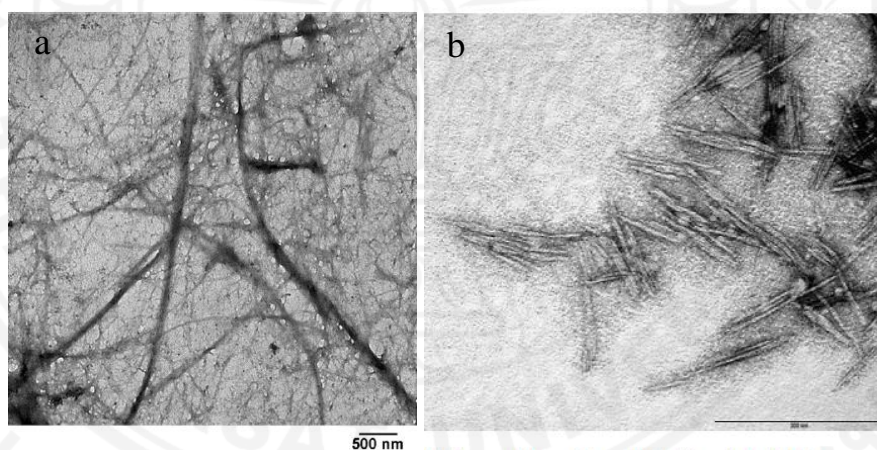
Figure 7 Transmission electron micrographs of (a) wheat straw nanofibers (Alemdar & Sain, 2008) and (b) eucalyptus cellulose nanowhiskers (Paula et al., 2011)

2.6.1 Preparation of cellulose nanocrystals

Cellulose nanocrystals (CNC) can be prepared by acid hydrolysis using sulfuric acid (H_2SO_4) or hydrochloric acid (HCl). Methods for preparation of CNC are not much different in each research work, as shown in **Table 2**. Nonetheless, acid types and hydrolysis times are very important. Gu, J., et al. studied sulfate esterification level of CNC, which was highly dependent on hydrolysis times and acid types. CNC were produced by hydrolysis of cotton

12

cellulose using sulfuric or hydrochloric acid, to compare the effects of types of acid. Sulfuric acid produced negative-charged sulfate, which leaded to more stable nanocrystals suspension. However, CNC prepared by hydrochloric acid had not possessed surface modification and detectable charges. Sulfuric acid is normally used to synthesize cellulose nanocrystals, since it produces more uniform particles and more stable suspensions. However, CNC produced from H_2SO_4 might exhibit negative properties for some applications. The introduction of sulfate groups leads to lower degradation temperatures, which may limit its implementation in thermoplastic composites (Gu et al., 2013).

Table 2 Preparation of cellulose nanocrystals derived from different cellulose sources

Cellulose sources	Acid hydrolysis condition					References
	Acid	Concentration	Ratio of Cellulose to Acid	Time (min)	Temp(°C)	
1. Cotton linters	H_2SO_4	65%	30 g / 35 ml	60	45	(Tehrani & Neysi, 2013)
2. Cotton silver	H_2SO_4	60%	1 g / 10 ml	60	60	(Hebeish et al., 2014)
3. Softwood pulp	H_2SO_4	64%	1 g / 10 ml	45	45	(Dash et al., 2013)
4. Cotton cellulose	H_2SO_4	63.5%	55 g / 500 ml	90	45	(Gu et al., 2013)
5. Wood pulp	H_2SO_4	65%	10 g / 160 ml	50	50	(Paula et al., 2011)
6. MCC from wood pulp	H_2SO_4	63.5%	55 g / 500 ml	90	45	(Guo & Catchmark, 2012)
	HCl	4M	5 g / 175 ml	225	80	
7. Cotton fiber	HCl	Concentrated	1 g / 20 ml	60	80	(Spagnol et al., 2012)
8. Bleached coconut husk fibers	H_2SO_4	64%	1 g / 10ml	120-180	45	(Rosa et al., 2010)
9. Ramie fibers	H_2SO_4	65%	-	30	55	(Raquez et al., 2012)
10. Pea hull fiber	H_2SO_4	64%	30 g / 250 ml	240-1440	45	(Chen et al., 2009)
11. Bamboo waste	H_2SO_4	64%	-	130	45	(Visakh et al., 2012)
12. Rice straw	H_2SO_4	64-65%	1 g / 8.75 ml	30 or 45	45	(P. Lu & Hsieh, 2012b)
13. Bleached sugar bagasse	H_2SO_4	6M	5 g / 100 ml	30 or 75	45	(Teixeira et al., 2011)
14. MCC (Commercial)	H_2SO_4	64%	1 g / 9.8 ml	120	44	(Gonzalez et al., 2014)
15. Bleached Sisal fiber	H_2SO_4	65%	-	15	60	(Rodriguez et al., 2006)

14

2.7 Biodegradable polymers

Biodegradable polymers have been developed for more than two decades. Biodegradable polymers can refer to both polymers that derived from nature and synthetic polymers (L. S. Nair & Laurencin, 2007). There are several types of biodegradable polymers such as natural biodegradable polymers (starch, cellulose, chitin, chitosan, etc.), polymers with hydrolyzable backbones (polylactide, polycaprolactone, polyurethanes, etc.), and polymers with carbon backbones (poly(vinyl alcohol), poly(vinyl acetate), polyacrylates, etc.). Biodegradable polymers seem to be more interesting materials because they can be degraded by natural processes that convert organic chemicals to simpler compounds through elemental cycles such as carbon, nitrogen, and sulfur cycles (Chandra & Rustgi, 1998).

2.8 Poly(lactic acid) or PLA

PLA is one of biodegradable polymers derived from sustainable resources such as corn starch or sugarcane. It is in a group of linear aliphatic polyesters, which can be produced from direct condensation polymerization of a basic bulding block of lactic acid or from a ring-opening polymerization of its dimer, lactide (Kalia et al., 2011). Lactic acid is produced by bacterial fermentation, followed by ring-opening or gradual condensation polymerization to form PLA with a mixture of D- and L-isomers. This can be degraded by natural process or simple hydrolysis of the ester bonds without the use of any enzymes. The rate of degradation depends on size, shape, isomer ratio of PLA, and temperature. The material has many interesting properties such as good mechanical strength, thermal plasticity, aesthetics, easy processability, and biocompatibility. However, PLA is brittle which is not proper for many applications (Awal et al., 2015; Garlotta, 2001).

The large-scale production of PLA products can be performed by injection molding, blow molding, thermoforming, and extrusion with adequate thermal stability to maintain molecular weight and prevent degradation. Thermal degradation of PLA occurs at the temperatures higher than 200 °C, which is depending on time, temperature, low-molecular weight impurities, and catalyst concentration (Garlotta,

2001). Solution cast method is used in small-scale productions. There are several types of solvents that are used to dissolve PLA pellet into solution form, such as chloroform or dichloromethane.
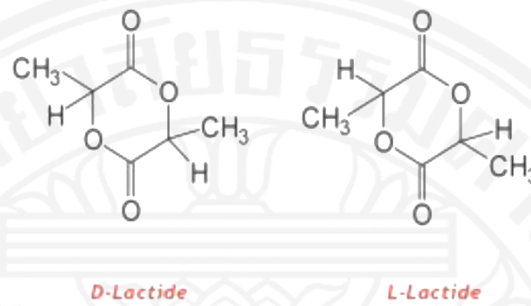
Figure 8 Structures of D-Lactide (left) and L-Lactide (right)(Rahamim, 2013)
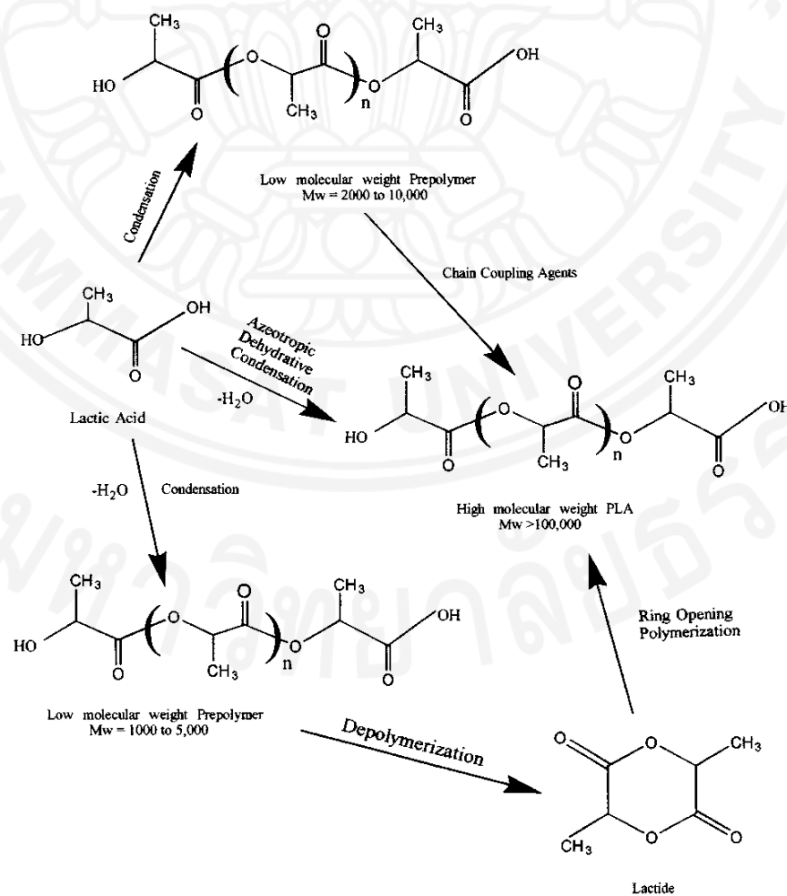
Figure 9 Synthesis methods for high-molecular-weight PLA (Garlotta, 2001)

2.9 Cellulose nanocrystals as bio- and nano-composites

Natural fibers, such as cellulose, have been used to reinforce various types of polymers because of their specific strengths and moduli, comparable to metals. The raw materials are derived from renewable resources and considered as green products. Cellulose fiber is commonly used in the preparation of green composites, due to its high strength and stiffness. However, since cellulose composes of glucose units which have high hydrophilicity, it can absorb significant amount of moisture. Thus, bubbles at the fiber surface are created at high temperature processing during evaporation, which can cause a reduction in degree of strong interaction in composites. Cellulose nanocrystals or CNC were used as biocomposites in various types of polymers., especially thermoplastic resins such as HDPE, LDPE, nylons, polyesters, PLA, and PVA. However, these polymers are mostly hydrophobic. Therefore, they do not well interact with cellulose fibers (Fakirov & Bhattacharyya, 2007).

Rubber/cellulose composites have been developed. Pasquini, D. et al. extracted cellulose nanowhiskers (CNWs) or rod-like cellulose nanocrystals from cassava bagasse, a by-product of cassava starch industrialization. The cellulose whiskers were prepared by sulfuric acid hydrolysis treatment. The results showed that cellulose whiskers with were high aspect ratio successfully obtained. Their potential as reinforcing agents for rubber matrix were studied, and the results showed improvements in mechanical properties (Pasquini et al., 2010). In similar approach, biodegradable polymers are considered in many research. The family of polylactides has significantly developed recently. Paula, E. L. P., et al. prepared bionanocomposites based on poly(D,L-lactide) and cellulose nanowhiskers (PDLLA/CNWs). The influence of the CNWs on the hydrolytic degradation behaviors of the polylactide was studied. Only 1% of nanofiller influenced a strong delay in the hydrolytic degradation of the PDLLA because the highly crystalline CNWs can inhibit water absorption, increase thermal stability, and increase the initial temperature of mass loss. These results indicated that only small amount of nanofillers significantly affects thermal stability and biodegradability of polylactides, which are good for preparing composites (Paula et al., 2011).

Another factor that influents the polymer's properties is the contents of CNWs added in PLA matrix. Lee, J. H., et al. varied CNWs compositions at 0.1 and 0.5 wt% and analyzed thermal stability, thermal behaviors, and mechanical properties of PLA/CNWs composite films. The results indicated that tensile strength and tensile modulus of the PLA composite films increased with an increase in the CNWs contents, as their high crystallinity promoted crystallization of the PLA matrix. However, the thermal stability of the composites decreased with the CNWs loading. The nanocellulose filler did not affect glass transition or melting temperatures of PLA matrix (Lee et al., 2013). However, increasing the amount of CNWs did not mean that the mechanical properties of the composites will increase. Hossain, K. M. Z. et al. varied the CNWs contents from 1, 3, to 5 wt% in PLA matrix and analyzed their physico-chemical and mechanical properties. The mechanical properties of the composites film reinforced by 1 wt% CNWs were better than others. This showed a 34 and 31% increase in tensile strength and modulus, respectively, compared to pure PLA. On the other hand, the dynamic mechanical analysis results showed that the tensile storage modulus also increased in the visco-elastic temperature region with increasing CNWs content in the nanocomposites. (Hossain et al., 2012).
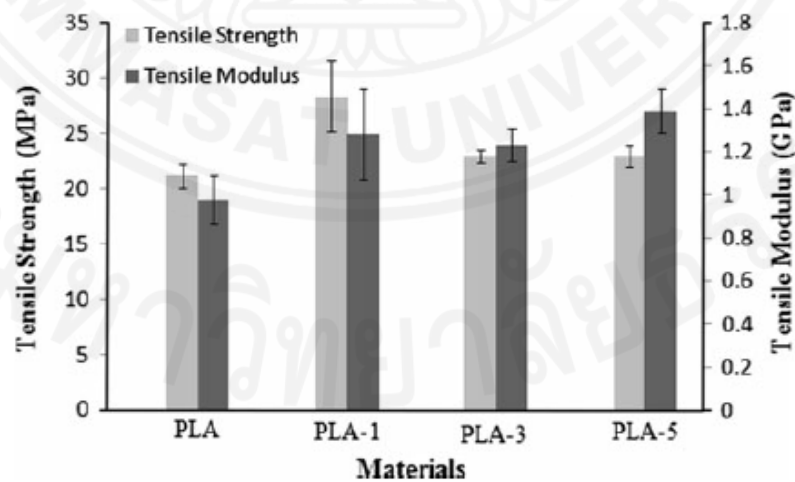
Figure 10 Tensile strength and modulus properties of PLA and nanocomposites
(Hossain et al., 2012)

Chapter 3
Methodology

3.1 Materials

Rice bran waste (RBW) was supplied by a rice bran oil production company in Nonthaburi, Thailand. Sodium hydroxide pellets (AR grade, Quality Reagent Chemical), Sodium Chlorite 80% (technical grade, Sigma-Aldrich), Acetic acid glacial with more than 80% acid by mass (Mallinckrodt Chemicals), Sulphuric acid (96%, Carlo Erba Reagents), Dichloromethane (Carlo Erba Reagents, France), Polyvinyl alcohol (M_w 9,000-10,000, Sigma-Aldrich) were used without further purification. PLA pellets purchased from NatureWorks LLC (Ingeo™ Grade 4043D, Density = 1.24 g cm^{-3}) were used as a matrix for the nanocomposites preparation.

3.2 Preparation of rice bran cellulose (RBC)

Preparation of RBC are divided into 2 steps, as described below:

3.2.1 Alkali treatment

The alkali treatment method was modified from that of Deepa et al. the rice bran waste raw material was by sieved at 180 mesh, and then purified by removing lignin and hemicellulose. 30 g of rice bran waste was treated with 750 ml of 4 wt% NaOH solution in an Erlenmeyer flask. The mixture was autoclaved with high pressure steam sterilizer (TOMY SX-700, Japan) as a sterilize liquid at 120 °C for 1 h. Finally, the remaining solid was filtered with electric aspirator (JEIO TECH, Korea) and neutralized by washing several times with excess distilled water (Deepa et al., 2011).

3.2.2 Bleaching treatment

The bleaching process was modified from that of LaCourse et a1. The alkali-treated sample was soaked in a 1 wt% aqueous chlorite solution. Acetic acid was then added to adjust the pH of the sulotion to 5±0.2 (SUNTEX SP-2200, Microprocessor pH meter, Taiwan). The mixture was

then heated to 80°C with constant agitation by a magnetic stirrer (IKA RCT basic, Malaysia) overnight, and the pH was checked for a few times to complete the reaction. When, the material's color turned to white, it was allowed to cool and then filtered by a suction filtration. The solid product was mixed with ethanol at a ratio of 1:3 (sample over liquor) for a few hours to remove the remaining water, before filtered and washed again with acetone. The product was finally oven dried in a hot-air oven (BINDER, Germany) at 50 °C overnight. Finally, a snowy white powder product was obtained (LaCourse et al., 1994).

3.3 Preparation of cellulose nanocrystals (CNC)

This process was modified from that of Lu and Hsieh. Bleached rice bran was treated by a concentrated sulfuric acid solution (64wt% sulfuric acid in water) at 45 °C for 45 min under constant stirring on a shaking incubator (Labnet, USA). The ratio of rice bran to acid solution was varied from 1–20 g/ml. The suspension was then diluted 10 times by deionized water, and kept in a refrigerator to prevent further reaction. Residual sulfuric acid in the suspension was then removed by repeated centrifugation (TOMY MX-305 High speed refrigerated micro centrifuge) at 10,000 rpm for 25 min. The supernatant (CNC suspension) and the precipitate (PREP) were collected and dialyzed with molecular porous membrane tubing at a molecular weight cutoff 12,000–14,000 (Spectrum Labs, USA) against deionized water for 4–5 days to remove the remaining acid, until it reached a constant pH. Finally, CNC was obtained in a deionized water solution (P. Lu & Hsieh, 2012b). The concentration was increased by removing water in the solution using a rotary evaporator (IKA HB 10, USA). Finally, the total solid or total carbohydrate of CNC was measured by using a sulfuric acid-UV method (Albalasmeh & Ghezzehei, 2013). First, the glucose standard at concentrations of 0, 0.2, 0.4, 0.6, 0.8, and 1 µg/mL were prepared for use in the construction of a calibration curve. Then, 1 mL of carbohydrate solution was mixed with 3 mL of concentrated sulfuric acid in a test tube and vortex for 30 s. the solution was cooled in ice for 2 min to bring it to room temperature. Finally, UV light absorption at 315 nm of the samples was measured by using UV/VIS spectroscopy.

3.4 Preparation of neat PLA and PLA/CNC composite films

In the preparation of nanocomposites, the method was modified from that of Johar et al. Solvent cast nanocomposites were prepared by dissolving PLA pellets in dichloromethane (5% w/v), in which the solution was stirred constantly using a magnetic stirrer at ambient temperature until the pellets were fully dissolved. Subsequently, CNC suspension with concentrations of 0.2 and 0.5 wt%, based on PLA pellets, were added and mixed thoroughly for 3 h. Polyvinyl acetate (PVA) was added as a surfactant at 0.2 wt% CNC content. After purging residual bubbles by sonication with an ultrasonic bath (Crest Ultrasonics, USA), the mixture was poured into Teflon trays to evaporate dichloromethane under ambient temperature. After 24 h, the resulting films were dried in a vacuum oven (BINDER, Germany) at 50 °C for 3 h to remove residual solvent (Johar et al., 2012).

3.5 Characterization

3.5.1 Determination of cellulose, hemicellulose, and lignin contents

Cellulose, hemicellulose, and lignin contents in RBW and RBC were determined by the TAPPI 203 om-88 standard (Maniaw, 2009), as detailed below:

3.5.1.1 Cellulose content

(1) 1.5 g of sample was placed in a 250-mL beaker and 100 mL of 17.5% NaOH reagent was added. The mixture was then stirred by magnetic stirring for 30 min. Note the time at which the reagent was added. After that, it was left at ambient temperature for 30 min.

(2) At the end of the 60-min period, the pulp suspension was stirred by a glass rod and transfered to a filtering funnel. The first 10 mL of the filtrate was discarded whereas the remaining 100 mL of the filtrate was collected in a clean and dry filtration flask.

(3) 10 mL of the filtrate and 10.0 mL of 0.5N potassium dichromate solution were pipetted into a 250-mL flask. Then, 50 mL distilled

water was added and mixed. Subsequently, 30mL concentrated H_2SO_4 solution was added cautiously, while swirling the flask.

(4) The solution was allowed to remain hot for 15 min before adding of 2 to 4 drops of Ferroin indicator. The mixture was then titrated with 0.1N ferrous ammonium sulfate solution to a purple color.

(5) A blank titration was conducted by substituting the filtrate with 5 mL of 17.5% NaOH solution. The cellulose content was calculated according to the following equation:

$$\text{Cellulose content (\%)} = 100 - [6.85(V_2 - V_1) \times N \times 20/(A \times W)] \qquad (1)$$

When V_1 = Titration of sample

   V_2 = Blank titration

   N = Exact normality of the ferrous ammonium sulfate solution

   A = volume of the filtrate used, mL

   W = Weight of sample

3.5.1.2 Lignin content

(1) 50.0 mL of the filtrate was pipetted into a 100-mL graduated cylinder having a ground glass stopper. 50.0 mL of 3N H_2SO_4 was added and mixed thoroughly by inverting.

(2) The cylinder was heated and submerged in a hot water bath at about 70-90°C for a few minutes. The precipitate was allowed to settle for several hours, preferably overnight, then it was decanted or filtered, if necessary, to obtain a clear solution.

(3) 10 mL of the clear solution and 10.0 mL of 0.5N potassium dichromate solution were pipetted into a 250-mL flask. Then, 50 mL distilled water was added and mixed. Subsequently, 30 mL of concentrated H_2SO_4 solution was add cautiously while swirling the flask.

(4) The solution was allowed to remain hot for 15 min before adding of 2 to 4 drops of Ferroin indicator. The mixture was then titrated with 0.1N ferrous ammonium sulfate solution to a purple color.

(5) A blank titration was conducted by substituting the filtrate with 5 mL of 17.5% NaOH solution. The lignin content was calculated according to the following equation:

$$\text{Lignin content (\%)} = 6.85(V_2\text{-}V_1) \times N \times 20/(A \times W) \tag{2}$$

3.5.1.3 Hemicellulose content

Hemicellulose content of the samples was calculated by using the following equation:

$$\text{Hemicellulose content (\%)} = 100 - (\% \text{ Cellulose} - \% \text{ Lignin}) \tag{3}$$

3.5.2 X-ray diffraction (XRD) analysis

The XRD patterns of RBW, RBC, CNC, and PREP were measured with 1.54 $ÅCuK\propto$ radiations at 40 kV and 30 mA. The scanning region of the two-theta angle (2θ) was conducted from 5° to 40° with a scan rate of 1°/min. (Bruker D8 Advance) (Neto et al., 2013).

For nanocomposite films, the diffraction patterns were recorded from 2°-50° with a step size of 0.04° and a scan step time of 2 s. (Hossain et al., 2012). The Crystallinity Index (Cr.I.) was determined by the following equation:

$$\text{Cr.I. (\%)} = (Sc \,/\, St) \cdot 100 \tag{4}$$

where: Sc is area of the crystalline domain

St is area of the total domain

(Ciolacu et al., 2010)

23

3.5.3 Thermogravimetric analysis (TGA)

TGA analyses were performed to observe thermal stability of materials (TGA, METTLER TOLEDO, USA). RBW, RBC, CNC, and PREP samples were weighted around 5-10 mg and placed in a clean ceramic plate, where the data were recorded by heating the samples at 10 °C/min from 30°C to 600 °C in N_2 atmosphere with a purging rate of 50 mL/min (P. Lu & Hsieh, 2012a). TGA measurement of nanocomposite films was conducted from 25°C to 500°, with the same heating rate and N_2 purging rate (Hossain et al., 2012).

3.5.4 Differential scaning calorimetry (DSC) analysis

Thermal behaviors and crystallinity of PLA in the nanocomposite films were examined by using DSC analysis (METTLER TOLEDO DSC822[e], USA). Samples were weighted about 6 mg and heated from -20 °C to 200 °C. The samples were subsequently cooled down to -20°C, with a cooling rate of 5 °C/min, before heating again to 200°C at the same heating rate. The percentage crystallinity (X_c) of all films were calculated by the following equation:

$$X_c[\%] = \frac{(\Delta H_m)/\phi_{PLA}}{\Delta H_m^0} \times 100\% \quad \quad (5)$$

where: ΔH_m is the enthalpy of fusion (J/g) of the polymer nanocomposites

ΔH_m^0 is the enthalpy of fusion of infinite size of pure PLA crystal (about 93.6 J/g)

ϕ_{PLA} is the fraction of PLA in the nanocomposites

(Hossain et al., 2012)

3.5.5 Fourier transform infrared (FTIR) spectroscopy

Chemical structures of RBW, RBC, CNC and PREP products were examined by fourier transform infrared (FTIR) spectroscopy (NICOLET 6700, Thermo Scientific, USA). The sample in powder form was grinded and mixed with KBr at a concentration of ca. 1 % wt. The mixture was then compressed

into a disc form by using a hydraulic machine at a pressure of 9.5 tons for 10 sec. All spectra were recorded from 4000-400 cm^{-1}, with 32 scans at a resolution of 4 cm^{-1}.

Interaction between components of the composite films were also characterized by FTIR with attenuated total reflection mode ATR-FTIR (Thermo Scientific, iD5). All spectra were recorded in the range of 4000-400 cm^{-1}, with 32 scans at a resolution of 2 cm^{-1}.

3.5.6 Scanning electron microscopy (SEM)

Morphology of all samples was examined on a HITACHIS-3400N scanning electron microscope, Illinois, USA with voltage of 30 kV. The cross-section morphology of the films were determined by breaking the sample after soaking in liquid nitrogen before.

3.5.7 Transmission electron microscopy (TEM)

The dimensions and shape of CNC samples were investigated on a JEM-2100 transmission electron microscope, JEOL, USA with an accelerating voltage of 80 kV(Johar et al., 2012). CNC samples were prepared by dropping into a copper grid and straining with 2% uranyl acetate, and dried at an ambient temperature before analysis.

3.5.8 Mechanical analysis

Mechanical properties of films, such as Tensile strength, Young's modulus, and Elongation at break were measured by using a Universal testing machine (H5KT, Tinius Olsen, UK). The samples were prepared to have 50 mm gauge length and 15 mm width. A cross head speed of 1 mm/min and a 1 kN load cell was employed in the measurements (Hossain et al., 2012).

3.5.9 UV-VIS Spectrometer

The concentration of CNC solution was measured by a UV-VIS spectrometer (Lambda 650, PerkinElmer, USA) at UV light absorption 315 nm.

3.5.10 Contact angle analysis

Hydrophilicity of the film's surface was examined by measuring their contact angle on contact angle instrument, Dataphysics, Germany.

3.5.11 Zeta sizer (Nano series)

Size and zeta potential of CNC were determined by Nano-ZS Zeta sizer (Malvern Instruments, UK)

3.5.12 Water vapor permeation analysis

Water vapor permeability of composite films were measured on a 7002 Water Vapor Permeation Analyzer (Illinois Instruments, USA). The measurement was performed at 38 °C and 90%RH.

3.5.13 Oxygen permeability analysis

Oxygen permeability of neat PLA film and nanocomposite films were measured by using OX-TRAN Model 2/21 Oxygen Permeability (Mocon, USA).

Chapter 4

Results and Discussion

4.1 Characterization of cellulose nanocrystals (CNC)

Chemical compositions of rice bran waste were determined from proximate analysis, as shown in Table 3. After alkali and bleaching treatments, the color of the rice bran waste (RBW) changed from brown to white color of rice bran cellulose (RBC), as shown in Figure 11. The purity or percentage of cellulose content in RBW and RBC were obtained from the TAPPI 203 om-88 standard. Then, RBC was hydrolyzed by sulfuric acid solution to obtain cellulose nanocrystals (CNC) solution, as shown in Figure 12. The precipitate (PREP) from acid hydrolysis was also collected, and its properties are characterized. All materials were characterized in terms of chemical, physicochemical, and morphological properties.

Table 3 Rice bran waste compositions (Appendix A)

Composition	Percentage (%)
Moisture	9.06
Protein	12.47
Fat	1.35
Ash	7.80
Total Carbohydrate	69.32
Dietary Fiber	27.14

Figure 11 Images of rice bran waste (RBW) (a) and rice bran cellulose (RBC) (b)

Figure 12 Images of precipitate (PREP) and cellulose nanocrystals (CNC) solution

From UV-VIS spectrometry, the concentration of CNC solution is about 5573 µg/mL. The percentage of cellulose, hemicellulose, and lignin in RBW and RBC samples after purification and the yield percentage of materials after each preparation steps is summarized in Table 4 and Table 5, respectively.

Table 4 Percentage of cellulose, hemicellulose, and lignin in RBW and RBC samples

Materials	% Cellulose	% Hemicellulose	% Lignin
RBW	82.7	9.2	8.0
RBC	87.0	8.2	4.8

Table 5 Yield percentage of products from each preparation steps

Methods	% Yield
RBW to RBC	4.9
RBC to CNC	2.9
RBW to CNC	0.1

28

4.1.1 Crystal structures analysis

The XRD traces of RBW and RBC samples are shown in Figure 13(a). In nature, these two patterns are typical of semicrystalline materials with an amorphous broad hump and crystalline characteristics with narrow sharp peaks (Ciolacu et al., 2010).

The calculated Cr.I. values of RBW and RBC samples are about 1.4 and 46.5%, respectively. The higher Cr.I. of cellulose is likely because of the reduction or partial removal of amorphous non-cellulosic domains induced by the alkali and bleaching treatments performed in the purification process. This is reflected by narrower and shaper peaks patterns (Johar et al., 2012). From Figure 13(b), the crystallinity of CNC slightly increases, compared to that of RBC since the acid hydrolysis treatment further removes additional amorphous components in the samples, leading to much sharper and more intense crystalline peaks with significant peaks located at 14.71°, 20.88°, 26.65°, with Cr.I of 47.8%. It is noted that during acid hydrolysis reaction, some of crystalline regions might also be removed (Haafiz et al., 2014). Cr.I of PREP was slightly higher than CNC (48.9%), because this also contains large particle's size of crystalline domains, which were separated and removed from small-size particles in the supernatant. This shows significant peaks at 20.9°, 21.46°, and 26.72°. From XRD results, RBW, RBC, and CNC samples can be classified as cellulose I or native cellulose because the diffractogram's profiles show characteristic signals at 15°, 17°, 21°, 23°, and 34° (Ford et al., 2010; Neto et al., 2013). This reflects of that acid hydrolysis did not affect the crystalline pattern of the samples (Johar et al., 2012).
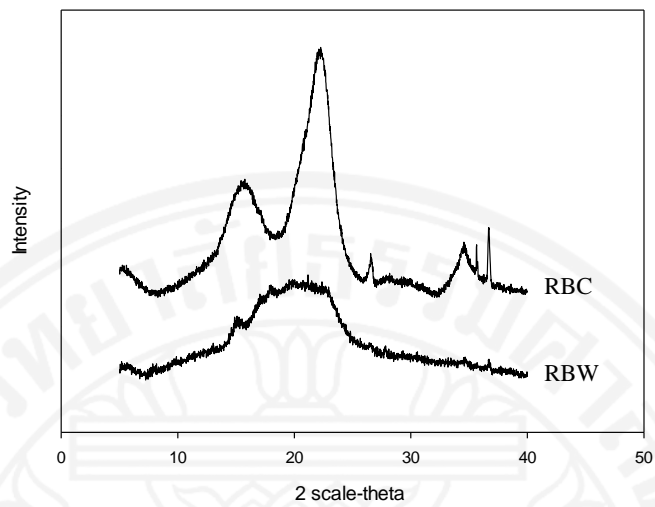
Figure 13(a) XRD patterns of rice bran waste (RBW) and rice bran cellulose (RBC)
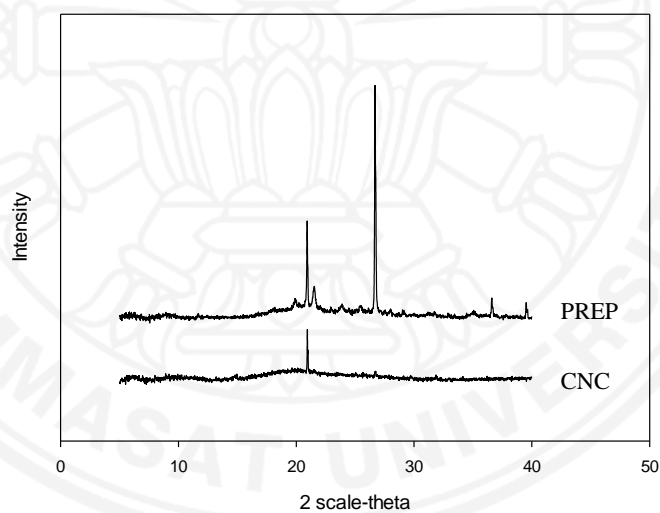
Figure 13(b) XRD patterns of cellulose nanocrystals (CNC)
and precipitate of CNC (PREP)

4.1.2 Thermal stability analysis

Thermogravimetric analysis is employed to observe and compare thermal behaviors of RBW, RBC, CNC, and PREP. Both RBW and PREP have four decomposition steps while RBC and CNC show only two and three decomposition steps, respectively. As shown in Figure 14(a) and (b), the small change in the first stage of massloss between 30-170°C is attributed to vaporization of moisture (Burhenne et al., 2013). The weight loss of RBW, RBC, CNC, and PREP in this step show comparable values at 9.32%, 7.31%, 9.47%, and 7.96%, respectively.

RBW has three steps of thermal degradation. First step is due to hemicellulose and cellulose decomposition because the difference in thermal degradation of cellulose and hemicellulose is not well-known. Since hemicelluloses are thermally the most unstable components of biomass, because of their random amorphous structures and reactive acetyl groups, the compounds decompose faster and at lower temperatures than lignin, with the onset temperature at around 161-249 °C and weight loss of 4.89%. The second step is mainly due to cellulose decomposition and some lignin at 248-358 °C, with 38.31% mass loss. The final step occurs at a temperature range of 359 to 487 °C. This reflects lignin decomposition, with a 11.77% weight loss (Ház et al., 2013; Jin et al., 2013; Rotliwala & Parikh, 2011).

Due to their homogeneity nature pertaining to linear chained structure of glucoses in cellulose, the RBC sample degrades in one step of the thermal degradation, at higher decomposition temperature, because lignin and hemicellulose have been removed during alkaline and bleaching treatments. Also, as some of the amorphous domains are removed from the sample, RBC has higher crystallinity so the material needs higher temperature to decompose, with approximate temperature range of 175 to 494°C (Jin et al., 2013).

The acid hydrolysis treatment has a profound effect on thermal stability of the samples. CNC shows the significant different properties, compared to others, especially the starting material RBC, i.e., the raw materials before acid hydrolysis reaction (Haafiz et al., 2014). These

differences might be a result from the presence of sulfate groups in the outer surface structure of the nano-crystalline particles (Wang et al., 2007). CNC also has lower degradation temperature, compared to RBW and RBC (111-190 °C of the first stage decomposition, which is depolymerization of cellulose). The initial temperature degradation is lower than that of RBC, likely because the sulfate groups influence more accessible of the degradation (Teixeira et al., 2011). Another stage of decomposition at 190 to 234 °C is due to the destruction unsulfated crystal strutures (Li et al., 2009). Additionally, PREP or the precipitate from acid hydrolysis treatment also has significant difference in thermal stability, compared to CNC. This might be because PREP consists of crystalline particles with different sizes, leading to multi-steps of decompositions. This is likely because of different contents of sulfate groups incorporated on the cellulose surface. The regions that contain lower sulfate contents degrade at higher temperatures, because of their higher thermal stability (Teixeira et al., 2011).

The final degradation is associated with ash formation. The residue of RBW and RBC are 35.54% and 23.74%, respectively. This is due to the lignin contents in the rice bran. Lignin has a tridimensional structure, in which its polymerization is randomly shared at the vegetable secondary wall. Therefore, its structure varies from one species to another. Even if the lignin is less stable than the cellulose, its degradation is very slow with the high rate of non-volatile products. Therefore, the mass loss of cellulose is higher than rice bran (Randriamanantena et al.). PREP has large amount of residues with a percentage of 54%. CNC shows the highest residue content of 59.1%, since sulfate groups act like a flame retardant or protective barrier attached on polymeric chains of the burning surface (Haafiz et al., 2014; Li et al., 2009). Sulfuric acid also acts as a dehydrating catalyst. After the evaporation of most of bound water at the temperatures below 100°C, the small amount of concentrated sulfuric acid generated homogeneously around the cellulose microfibrils. When heated to above 120°C, the reaction of $C_n(H_2O)m \rightarrow mH_2O + nC$ occurs, in which the sulfuric acid extract water molecules from the cellulose structure and evaporate immediately. Therefore, oxygen atoms

that are removed in the form of water would effectively prevent weight losses because of less carbon combustion (Kim et al., 2001). Moreover, due to the small particle size of CNC, The material has a high number of free end chains, which can decompose at higher temperatures (Wang et al., 2007). From this increased thermal stability, CNC can potentially be used as reinforcing agent to increase thermal stability of bio-composites materials.
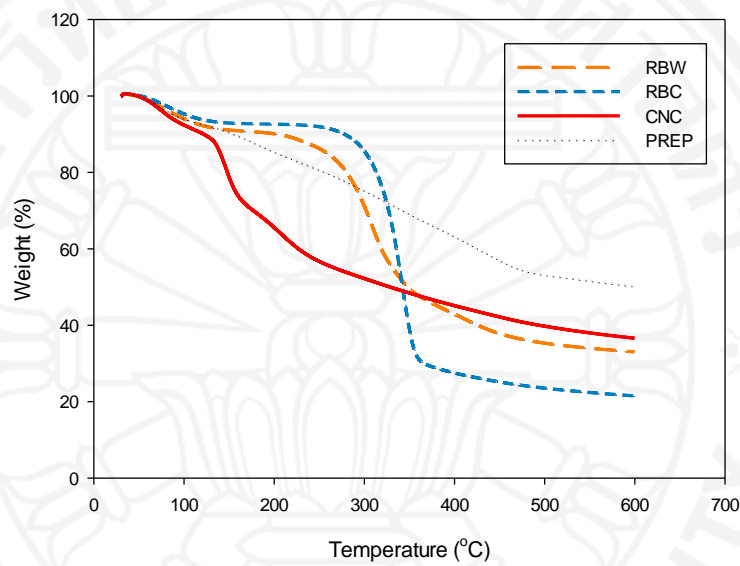
Figure 14(a) TGA curves of RBW, RBC, CNC, and PREP
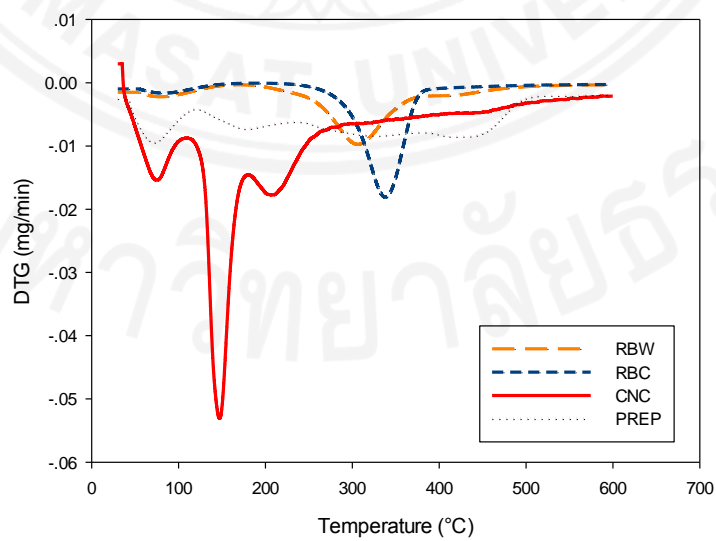
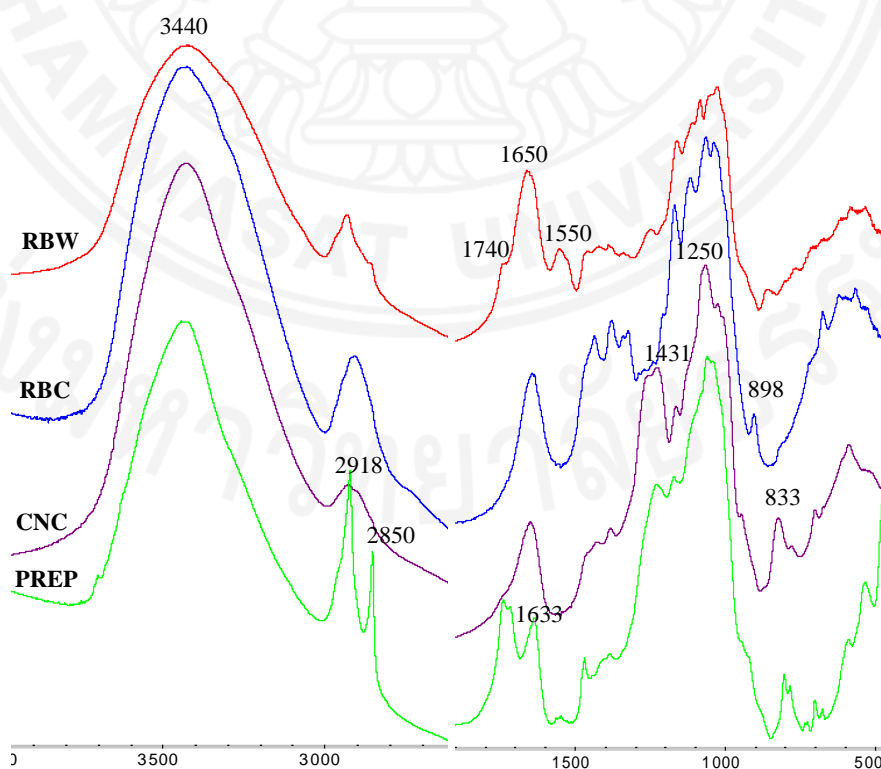**Figure 14(b)** DTG curves of RBW, RBC, CNC, and PREP

4.1.3 Chemical structures analysis

Chemical structures of RBW, RBC, CNC, and PREP samples are examined by FTIR spectroscopy. The spectra of these samples are compared in Figure 15. A broad band enveloped the 3440 cm^{-1} region, observed in all samples, represents the stretching mode of -OH groups. The signals located in the region of 2920-2910 cm^{-1} correspond to C−H stretching vibration of cellulose (Haafiz et al., 2014). The strong band located at around 1650 cm^{-1} in all spectra is associated with a bending mode of −OH groups in the structures of cellulose or bound water in the compound. CNC has the highest intensity of this mode compared to others, indicating its relatively higher degree of purity of cellulose (Johar et al., 2012). In addition, a medium-to-weak band is observed as a shoulder peak at 1740 cm^{-1}, due to the C=O stretching mode of ester groups in hemicellulose or carboxylic acid groups in the ferulic and p-coumeric components of lignin. The intensity of this mode is relatively stronger in RBW compared to CNC and RBC, indicating that these functional groups are separated from the 2 components during the extraction process. In contrast, this vibrational mode presents as a separate strong band in PREP, reflecting a domination of this functional group. This reflects that the precipitate from the acid hydrolysis mainly consists of non-cellulosic constituents that are not hydrolyzed by the hydrolysis reaction. In addition, the PREP spectrum also exhibits other strong and sharp bands due to these non-cellulosic constituents at 2918, 2850 cm^{-1} (-CH stretching), 1633 cm^{-1} (unsaturated C=O stretching), and 802, 782 cm^{-1} (aromatic ring vibration).

The peak located at 1550 cm^{-1} is due to the presence of lignin, which is attributed to the C=C vibrational mode (Neto et al., 2013), or a bending mode of −NH groups likely from protein structures. As the peak disappears in the spectra of other products after alkaline and bleaching treatments. This indicate that can the treatments leads to a removal of noncellulosic materials (Johar et al., 2012; Trachea et al., 2014). The band observed in RBC, CNC, and PREP spectra at 1431 cm^{-1} indicates formation of intermolecular hydrogen bonding at C$_6$ group, which is confirmed by their higher cellulose contents (Haafiz et al., 2014; Trachea et al., 2014).

All spectra show bands at 1372-1383 cm^{-1}, due to a bending vibration of the C−H and C−O groups of saccharide rings. The signals at 1154–1163 cm^{-1} correspond to C−O−C asymmetric stretching and the board peaks around 1079-1112 represent C−O−C glycosidic ether linkages of hemicellulose or lignin (Silvério et al., 2013). The peaks at 1060 and 898 cm^{-1} are derived from C–O stretching and C–H rock vibrations of cellulose. The growth of these peaks represents the increase in the percentage of cellulosic components. The results indicate that after chemical treatments, the sample has higher cellulose contents or almost pure cellulose. (Haafiz et al., 2014; Neto et al., 2013; Silvério et al., 2013).

Interestingly, both CNC and PREP samples show a band associated with sulfate groups at 1250 cm^{-1}, which is due to the asymmetric S−O vibration, and the symmetric C−O−S vibration at 833 cm^{-1}. This is likely because there are some sulfate groups attached to the molecular surface of the samples during the acid hydrolysis, in which sulfuric acid was employed (Gu et al., 2013).

Figure 15 FTIR spectra of RBW, RBC, CNC, and PREP

35

4.1.4 Morphological properties

The morphological structures of all samples are investigated, as shown in Figure 16. RBW has agglomerated irregular fibrils shape, with rough surface morphology. After the alkaline and bleaching treatments, the morphology changed to be rod-like structures, as can be seen in Figure 16(b). RBC image suggests partial removal hemicellulose and lignin impurities after the chemical treatments, which are the cementing components around the fiber-bundles. As a result, only cellulose remained in the sample (Rosa et al., 2010).

During the alkaline treatment, it is expected that mainly hemicellulose is removed, while the bleaching treatment remove the rice bran fiber-bundles, and separate then into individual fibers. After the chemical treatments, the diameter of the fibers decrease from 40-580 μm to 40-300 μm. The size reduction is mainly attributed to the separation of the fibers' primary cell wall, due to the removal of hemicellulose and lignin. It is noted that RBC also has higher fiber aspect ratios, (length/diameter) around 2.40-9.17, compared to 1.0-2.4 in RBW (Johar et al., 2012).

The morphology of CNC and PREP is shown in Figure 16(c) and 16(d). The results indicated that the agglomeration is broken down after the acid hydrolysis. CNC has both fibrillar and spherical structures, which posseses further reduction in size and diameter, compared to RBC with the diameter of 15-200 μm and high aspect ratio around 1.0-35.0. The materials also have small amount of aggregation with irregular shape (Alemdar & Sain, 2008; Haafiz et al., 2014). PREP exhibits irregular morphology, which is different from CNC or the supernatant from the acid hydrolysis. The diameter is significantly similar to CNC but it has much lower aspect ratio about 1.0-6.0 This is perhaps because the precipitate contains crystalline regions with varied sizes and some of non-cellulosic constituent, which cannot be removed by the acid hydrolysis. In contrast, the supernatant contains crystalline cellulose or cellulose nanocrystals with smaller sizes, and these are materials of our interested. These results suggest that the increased property of CNC should provide higher reinforcing capability of the fibers for composite applications.

Figure 17 shows TEM image of CNC and PREP. Figure 17(a), confirms that the size of CNC is reduced to nano-scale at around 77-577 nm, with the uniform needle-like shape, as the amorphous region of cellulosic microfibrils are removed during the acid hydrolysis, leaving only straight crystalline domains (Johar et al., 2012). On the other hand, PREP has a large agglomerated structure of larger size crystalline domains with irregular shapes, leading to different morphology compared to CNC.
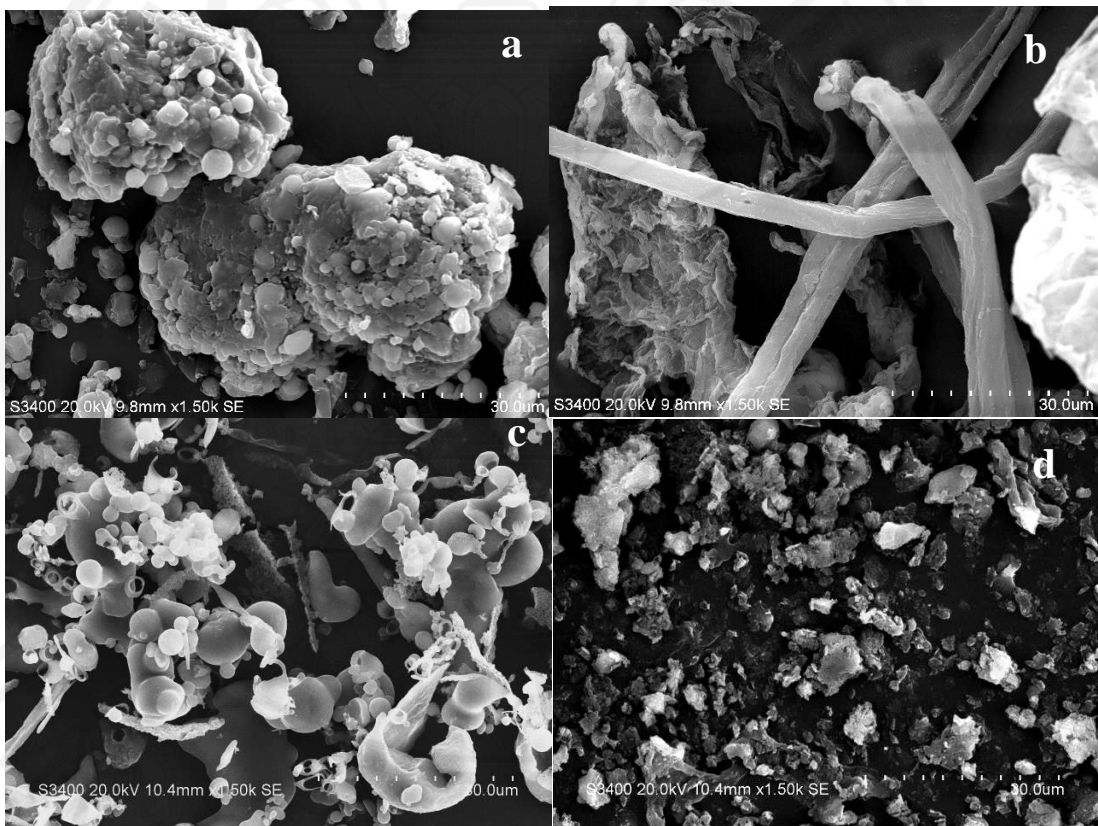
Figure 16 Scanning electron (SEM) micrographs of RBW(a), RBC(b), CNC(c), and PREP(d)
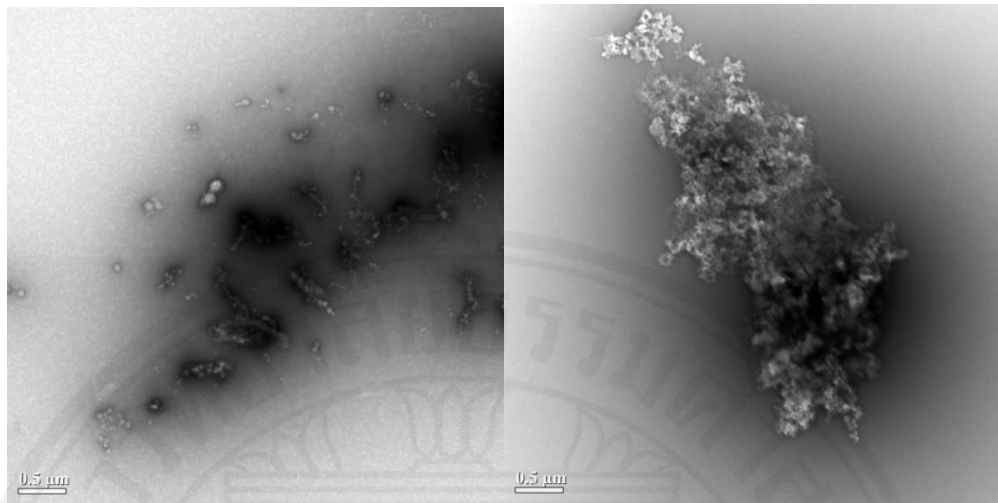
Figure 17 Transmission electron (TEM) micrographs of CNC(a) and PREP(b)

4.1.5 Size and zeta potential measurements

Information on Zeta potential is used to determine the stability of dispersed particles in a specific medium. It is a potential difference between the dispersion medium and the stationary layer of fluid attached to the dispersed particles. The results indicate that the zeta potential of CNC in water is about -21.9 ± 0.42 mV, which reflects incipient instability. The average size is about 897 ± 10.8 nm (Chang et al., 2015).

4.2 Characterization of neat PLA film and nanocomposite films

The obtained CNC is used in the preparation of PLA/CNC composites materials, to generate bio-based composites with improved mechanical properties, good degradability, and biocompatibility. All film samples were prepared by a solution cast method. Dichloromethane was used as solvent to dissolve PLA pellets. CNC, which is dispersed in water, were used as reinforcing agent, with 0.2 wt% and 0.5 wt% contents. The addition of PVA solution as a surfactant was used, enhance the CNC dispersibility in PLA solution. The images of neat PLA film and nanocomposite films are shown in Fig. 18. There are three composite films of 0.2 wt% CNC with PVA (0.2CNC-PVA), 0.2 wt% CNC without PVA (0.2CNC), and 0.5 wt% CNC

(0.5CNC), as shown in Figure 18(b), (c), and (d), respectively. The results suggest that after CNC was added into PLA solution, the water-based CNC solution did not well disperse in the oil-phase PLA solution. Therefore, two phases of water and dichloromethane cannot be well mixed, leading to bubbles formation and opaque zones in the resulting films after solvent evaporation. When the amount of CNC increases, the dispersion is lower and cause more opaque area. However, the addition of PVA surfactant influences better dispersion, resulting in a formation of film with improved homogeneity, i.e. less opaque zones, as shown in Figure 18(b). These films were further characterized in terms of mechanical properties and other specialized properties.
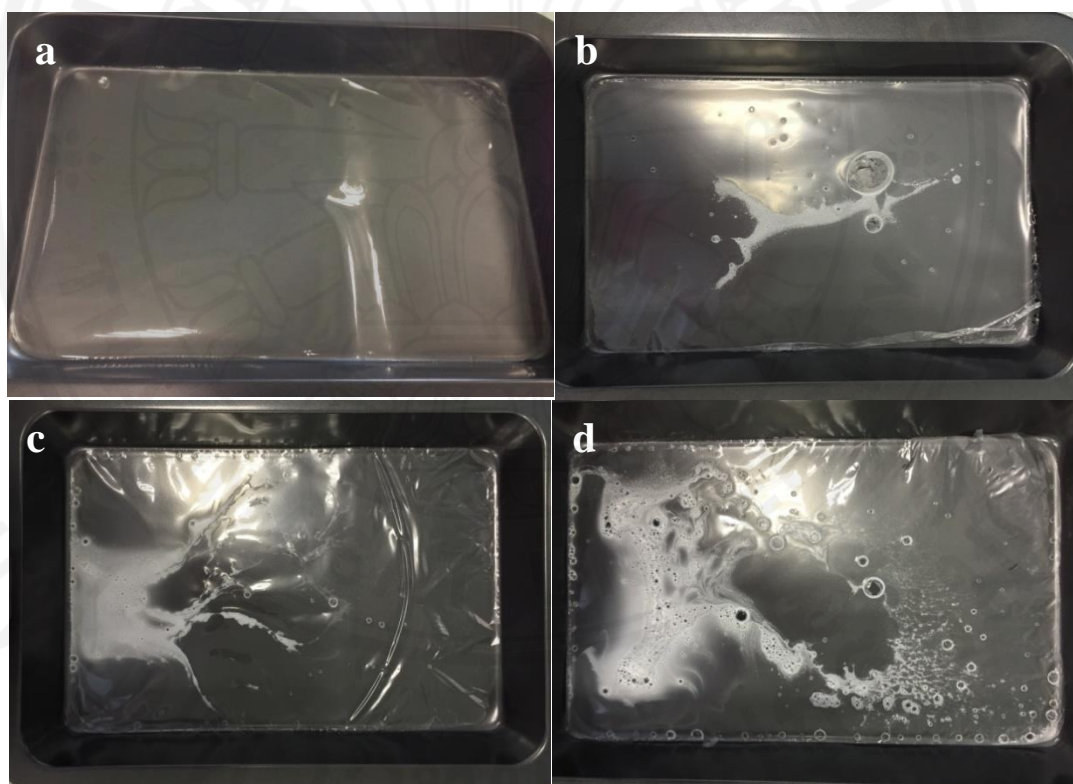
Figure18 Images of neat PLA(a), 0.2CNC-PVA(b), 0.2CNC(c), and 0.5CNC(d) films after solvent evaporation.

4.2.1 Mechanical properties

The mechanical properties of neat PLA film and composites film such as tensile strength, Young's modulus, and elongation at break are examined. Figure 19(a) shows the tensile strength of neat PLA and different composite films. The results show that only the 0.2 wt% CNC-PVA film has higher values of tensile strength (~45 MPa), with the percentage increase 3%, compared to neat PLA (~42 MPa). This is due to the better dispersion of CNC in the polymer matrix, when PVA surfactant is added. However, at 0.2 wt% and 0.5 wt% CNC content, the strong self-aggregation with random orientation of CNC leads to a decrease in tensile strength of the films (Hossain et al., 2012).

Figure 19(b) shows Young´s modulus of all films. 0.2CNC-PVA and 0.5CNC samples show similar percentage increase of roughly 6%. On the other hand, Young´s modulus of 0.2 wt% CNC is lower than neat PLA because of poor dispersion of CNC in the polymer matrix.

As shown in Figure 19(c), the percent elongation of all nanocomposite films, especially with 0.2CNC and 0.5CNC, significantly increase about 27% and 25%, respectively, compared to neat PLA. This reflects that the composite films have higher ductility, due to the presence of CNC, which can form strong interaction with the PLA matrix.
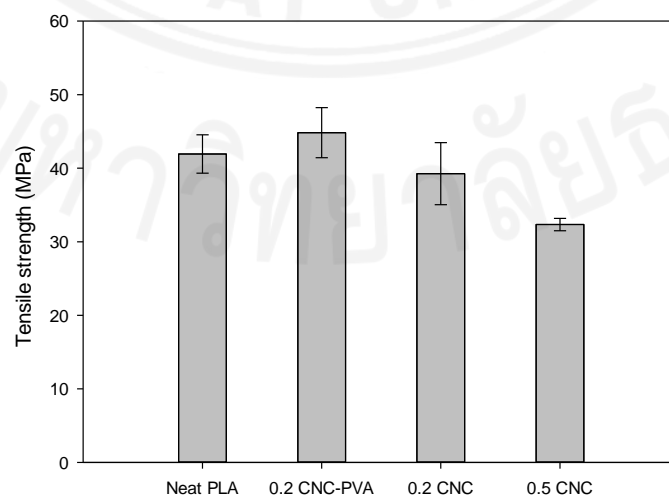
Figure 19(a) Tensile strength of neat PLA and composite films
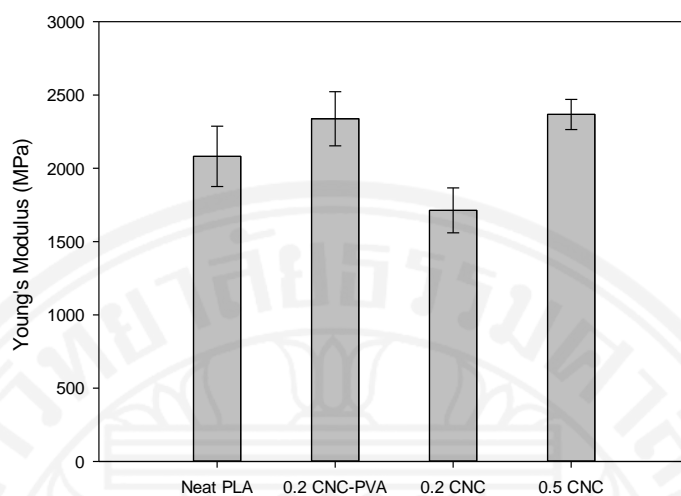
Figure 19(b) Young's modulus of neat PLA and composite films
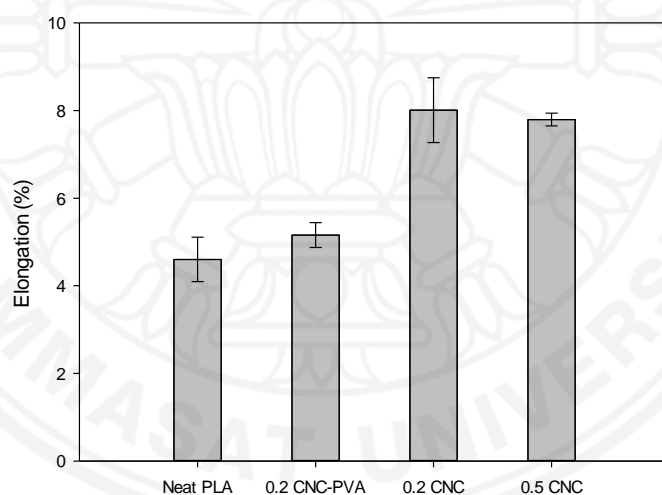
Figure 19(c) Elongation at break of neat PLA and composite films

4.2.2 Crystal structures analysis

The crystal structures of PLA and nanocomposite films were investigated by X-ray diffraction. Neat PLA shows significant peak only at 2θ = 16.9 while other patterns show significant peaks at 2θ = 15°, 16.9°, 19.3°, and 22.5° which represent the CNC in the composites. There are narrow sharp peak of crystalline with highest peak in all patterns at 2θ = 16.9° and the

intensity of this peak increased when CNC is added into the polymer matrix. 0.2CNC-PVA shows the best crystal structure with highest peak intensity since PVA can influence the better dispersion and interaction between CNC and PLA. Furthermore, 0.2CNC and 0.5CNC also show narrow sharp peaks that means the crystallinity is increased in nanocomposites (Hossain et al., 2012).

The crystallinity of all films are calculated and summarized in Table 6 The crystallinity values of each film before and after tensile testings i.e., original films and those stretched beyond the elongation at break point, are compared. All films show significant decrease of crystallinity after mechanical testing.
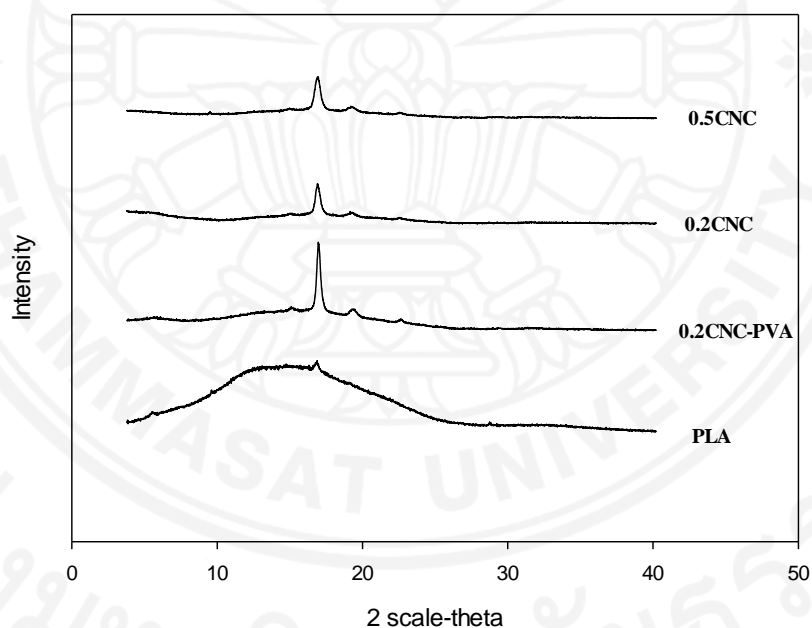
Figure 20 XRD patterns of neat PLA and composite films

Table 6 Crystallinity of film samples obtaibed from X-ray diffraction before and after mechanical testings.

Samples	Crystallinity (%)	
	Before	After
PLA	0.9	1.1
0.2CNC-PVA	20.1	0.9
0.2CNC	18.4	4.3
0.5CNC	28.6	5.2

4.2.3 Thermal behaviors and thermal stability analysis

DSC thermogram of all films are shown in Figure 21(A) and (B) which are neat PLA, 0.2 wt% CNC with PVA as a surfactant (0.2CNC-PVA), 0.2 wt% CNC (0.2CNC), 0.5 wt% CNC (0.5CNC), and 0.5 wt% CNC in opaque zone or the area that contains higher amount of CNC (0.5CNC_OP). The first heating scan provides information on ordered structure formation of specimens during the solvent casting process. As shown in Table 5, the glass transition temperature (T_g) of neat PLA and nanocomposite films are significantly different from one another, it might due to the preparation step. The crystallization temperature (T_c) and heat of crystallization (ΔH_c) occurs because the crystal cannot be formed completely when solvent evaporated. 0.5CNC has the highest T_c with the temperature of 116.8 °C because it contains highest amount of CNC, which can increase the crystallinity in PLA matrix. 0.2CNC-PVA also has higher T_c than 0.2CNC since PVA can influence CNC to have better dispersion to the solution so CNC can better interact with PLA matrix. It has the lowest ΔH_c and the smallest interval of onset and endset temperature which means PVA can help the composite film to be well defined. The melting temperature (T_m) of almost nanocomposites is slightly higher than neat PLA except 0.2CNC-PVA that has nearly the same result because the increasing of crystallinity from CNC slightly affects to increase T_m. The heat of fusion or ΔH_m of nanocomposties significantly increases from neat PLA due to higher crystallinity. Therefore, it needs higher energy to melt all crystalline. ΔH_m-ΔH_c of all samples are comparable. The results show that 0.2CNC-PVA, 0.2CNC, and 0.5CNC_OP have the highest values, since 0.5CNC has the highest ΔH_c. This is because the crystallization rate of composite films is slower than the cooling rate of DSC (Ehrenstein et al., 2004).

The second heating scan in Figure 21(B) shows only characteristic properties of the material (after controlled cooling). T_g of nanocomposite films slightly increases compare to neat PLA because of better interaction between OH group of CNC and carbonyl group of lactate. T_m also increases insignificantly with higher intensity when the amount of CNC increases since

nanocomposites has better degree of perfection which had greater chain fold or lamellar thickness in the structures. The cold crystallization or T_c is the crystal that formed from cooling run and the temperature slightly increases as increasing CNC content. ΔH_m-ΔH_c of all films in second scan are much lower than first scan and slightly lower than neat PLA. This is because cooling rate directly influences crystallization behavior and the rate is too fast to form perfect crystals (Ehrenstein et al., 2004; Hossain et al., 2012).
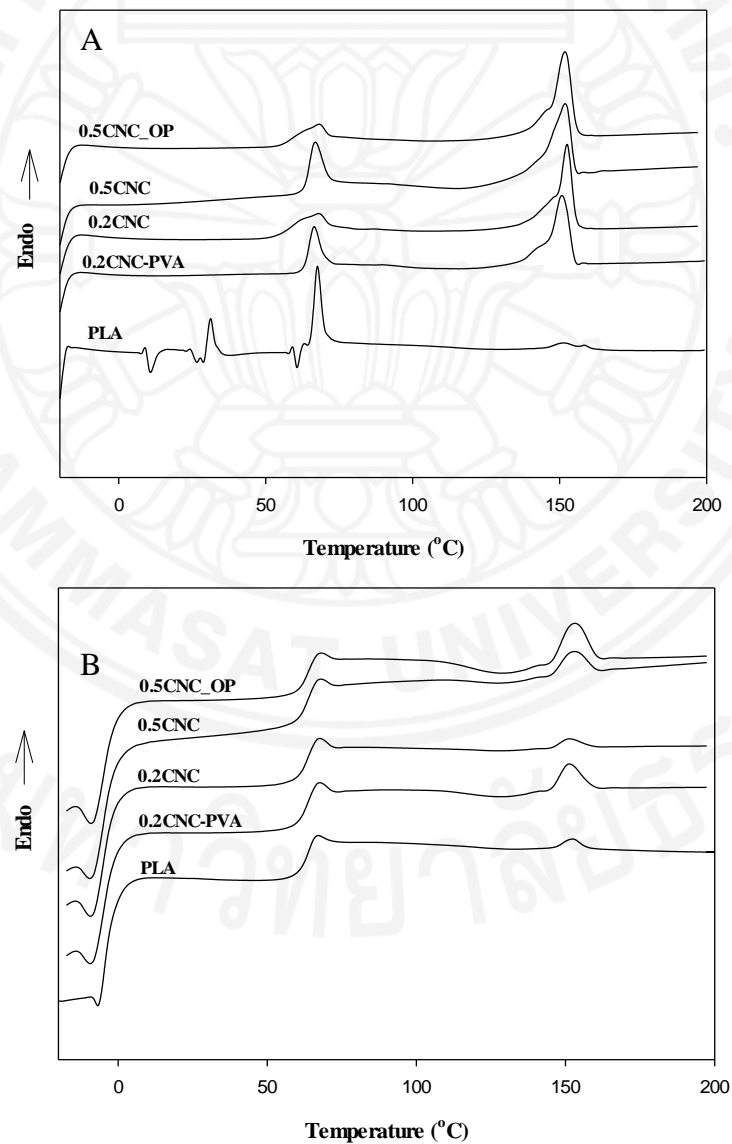
Figure 21 DSC thermograms of neat PLA and composite films from first heating run (A) and second heating run (B)

Table 7 DSC data obtained from the first heating run

Materials	T_g (°C)	T_c (°C)	T_m (°C)	ΔH_c (J/g)	ΔH_m (J/g)	ΔH_m-ΔH_c (J/g)
PLA	69.6	-	151.5	-	2.9	2.9
0.2CNC-PVA	62.9	114.1	151.2	5.3	16.0	10.7
0.2CNC	58.8	108.0	153.0	6.3	17.5	11.2
0.5CNC	63.2	116.8	152.3	12.0	17.2	5.2
0.5CNC_OP	64.0	109.2	152.0	7.0	19.7	12.7

Table 8 DSC data obtained from the second heating run

Materials	T_g (°C)	T_c (°C)	T_m (°C)	ΔH_c (J/g)	ΔH_m (J/g)	ΔH_m-ΔH_c (J/g)
PLA	62.8	-	152.3	-	1.0	1.0
0.2CNC-PVA	63.6	128.7	152.3	2.0	2.6	0.6
0.2CNC	62.8	-	152.7	-	0.9	0.9
0.5CNC	63.6	129.7	153.0	1.9	2.2	0.3
0.5CNC_OP	63.6	129.0	153.3	4.0	3.9	0.0

Figure 22(a) shows TGA thermograms of neat PLA and composite films. The onset of decomposition temperatures of nanocomposites appear at higher temperatures (312°C) than that of the neat PLA film (300°C). The derivative thermogravimetric (DTGA) curves are shown in Figure 22(b). The center of the degradation, reflected by the peak temperature, of a neat PLA film is around 360°C, while that of nanocomposite films is located at 366°C. This is in good agreement with other work reported in the literatures (Hossain et al., 2012; Petersson et al., 2007). The results suggest that the introduction of CNC to PLA matrix leads to a formation of stronger interation between CNC and PLA. This results in a slight increase in the thermal stability of the composites, reflecting by the increase in the onset and degradation temperature of the composite samples. However, the weigth loss percentage of all films are similar to one another at 96-97%, and the residues were around 3-4%, as only small amount of CNC is added.
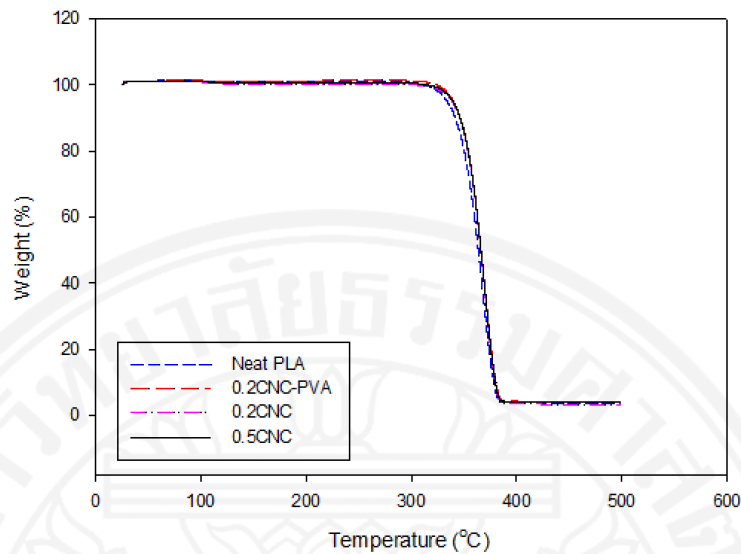
Figure 22(a) TGA curves of neat PLA and nanocomposite films
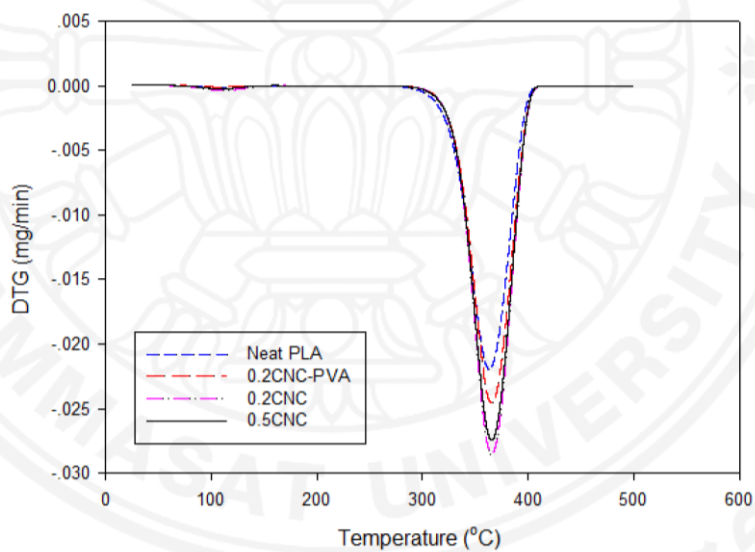
Figure 22(b) DTGA curves of neat PLA and nanocomposite films

4.2.4 Analysis of chemical structures and interactions

The chemical stuctures and intereactions between the components of the composites are examined by ATR-FTIR analysis, as shown in Figure 23. The result from these spectra provide information on the surface of the film samples. The vibrational mode at 3300 cm^{-1} is due to the –OH stretching mode of hydroxyl groups from CNC. The spectrum of neat PLA does not

exhibits this band, due to its low –OH content. All composite films, however, show broad band in this region, reflecting the presence of CNC at the film surface. This is in concert with an appearance of a broad band around 1700-1580 cm^{-1} in the composites samples.

The band at 1746 cm^{-1} in all films represents the C=O stretching mode of PLA. This band in nanocomposites slightly shifts to lower wavenumber, which is likely due to formation of strong hydrogen bonding interaction between PLA and CNC. A band located at 1042 cm^{-1} is associated with the C–O groups in the saccharide's structure. The intensity of this mode increases in the spectra of nanocomposite samples as CNC is incoporated. The signal at 920 cm^{-1} represents -CH$_3$ rocking mode of crystaline phase of PLA. The intensity of this band increases with the addition of CNC into the PLA matrix, reflecting higher crystallinity. In addition, a 755 cm^{-1} band, attributed to crystalline phase of PLA, also increases in the intensity in all nanocomposites compared to neat PLA (Auras et al., 2010; Hossain et al., 2012).
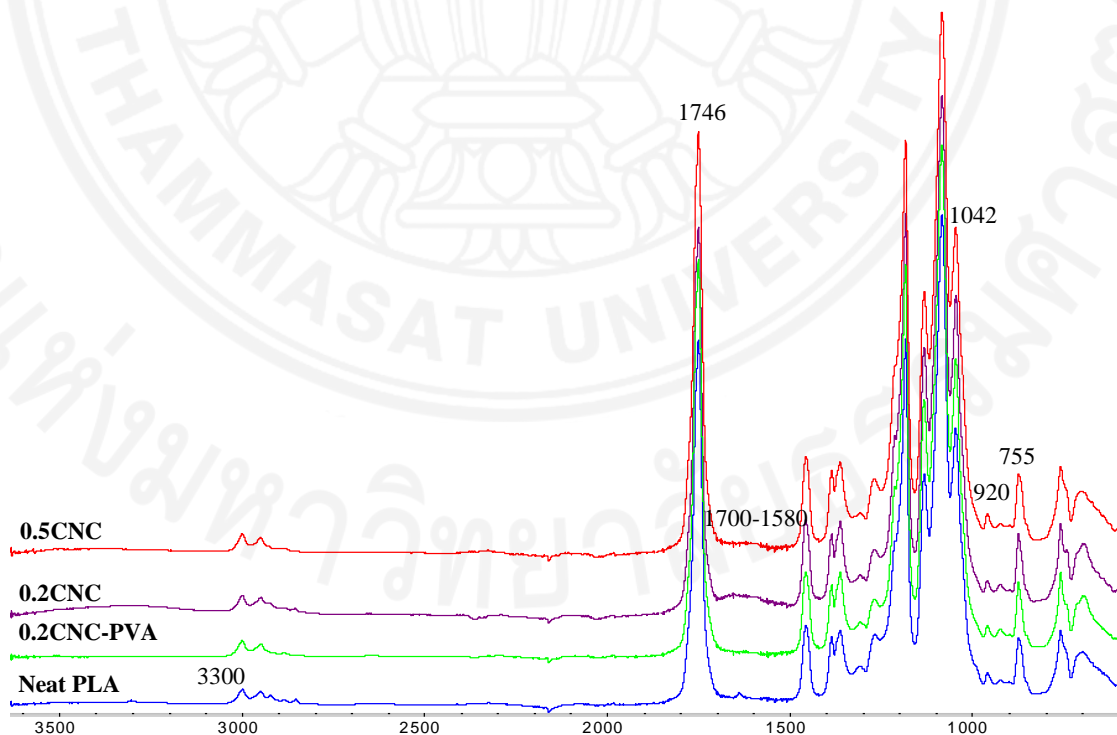
Figure 23 FTIR spectra of neat PLA and nanocomposite films

4.2.5 Morphological properties

The cross section morphology of films obtained from breaking of the samples in liquid nitrogen, are compared to investigate synergetic properties of the samples. The results clearly show morphological differences between neat PLA and nanocomposites. Neat PLA had smooth breaking surface, due to its brittleness nature, while nanocomposite films show rough fracture surface with some fibrillar fracture patterns, as observed in Figure 24(c) and 24(f). This confirms that there are CNC dispersed in the PLA films, leading to improvement in tensile strength and modulus of the composites, as previously described. This is because the CNC fibers can form stronger interaction with PLA.
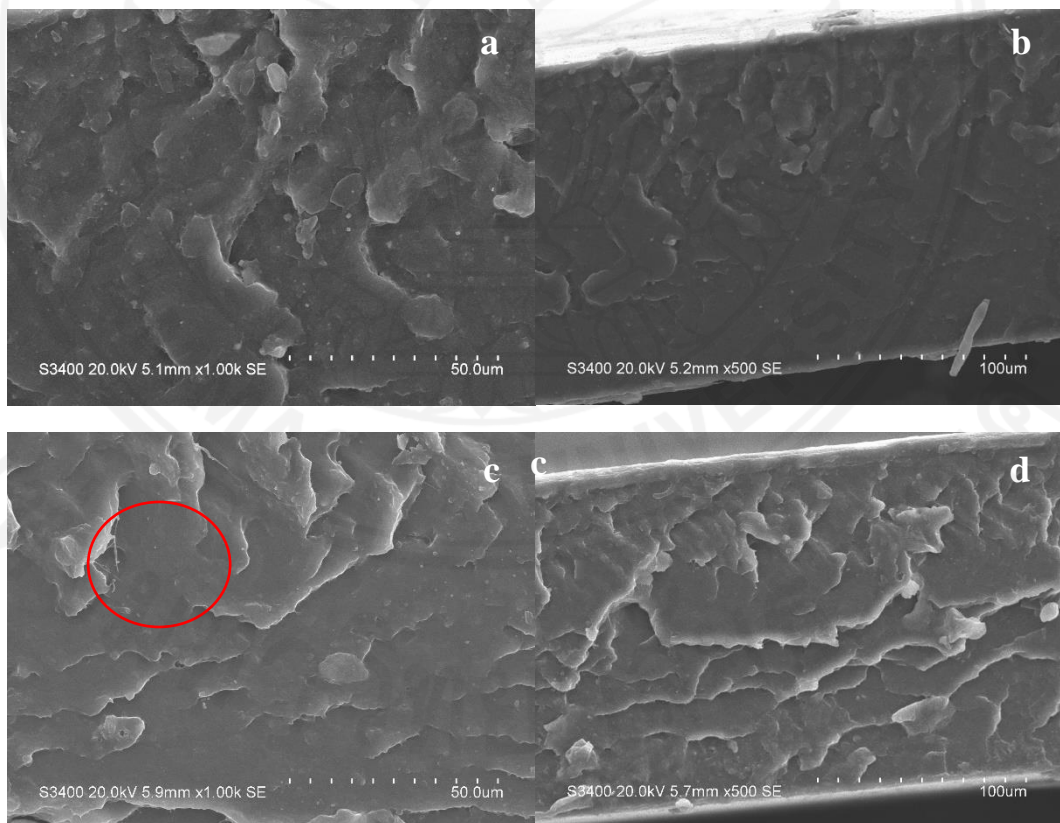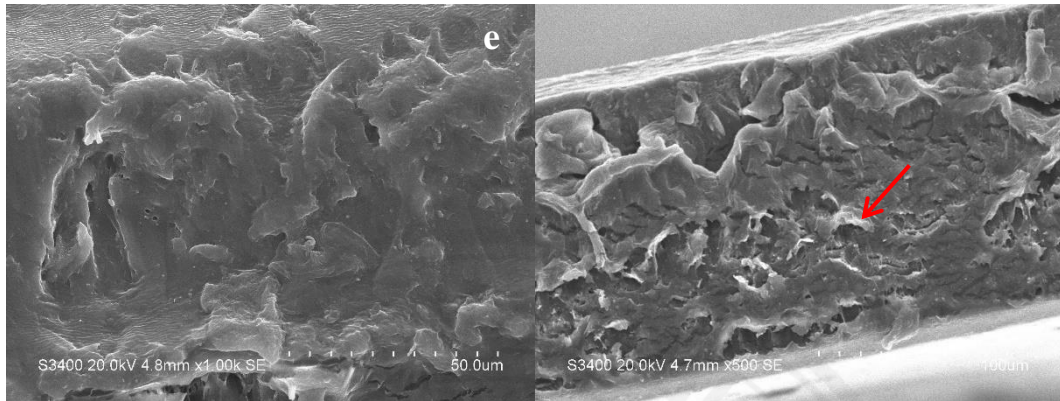
Figure 24 SEM images of cross section of neat PLA (a, b), 0.2CNC (c, d),
and 0.2CNC-PVA (e, f) films

The surface morphology of solvent cast films are also examined by SEM, as shown in Figure 25. As the composites samples contain transparent and opaque zones in the same films, these are examined separately to obtain insights into the origin of this difference. The surface of all composites have higher degree of roughness, compared to neat PLA. Composites containing CNC exhibit some regular shape particles on the surface of the transparent zone. This likely due to some of CNC particles, which migrate to the surface of films during the solvent casting step. However, the 0.2CNC-PVA sample, as shown in Figure 25(b) show smooth film surface, compared to its 0.2 CNC, without PVA. This confirms that PVA can promote compatibility of the CNC and PLA, which prevent the migration of CNC to the film surface. This leads to the presence of CNC inside the film matrix. The results also indicate that transparent zone of each composties are more homogeneous than the opaque zones, in which surface pores are observed, as shown in Figure 25(c) and (g). This porous pattern occurred due to the evaporation of water bubbles in the films during the casting step, as small amount of water used in the stabilization of CNC, phase separate from the PLA solution phase.

S3400 20.0kV 10.3mm x300 SE 100um

S3400 20.0kV 9.6mm x300 SE 100um

S3400 20.0kV 9.3mm x300 SE 100um

S3400 20.0kV 9.8mm x300 SE 100um

S3400 20.0kV 9.7mm x300 SE 100um

S3400 20.0kV 9.9mm x300 SE 100um
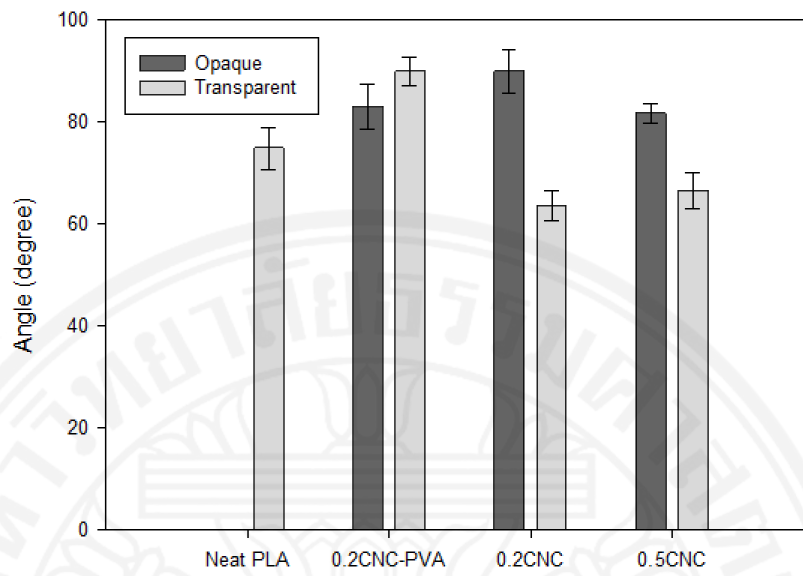
S3400 20.0kV 9.6mm x300 SE 100um
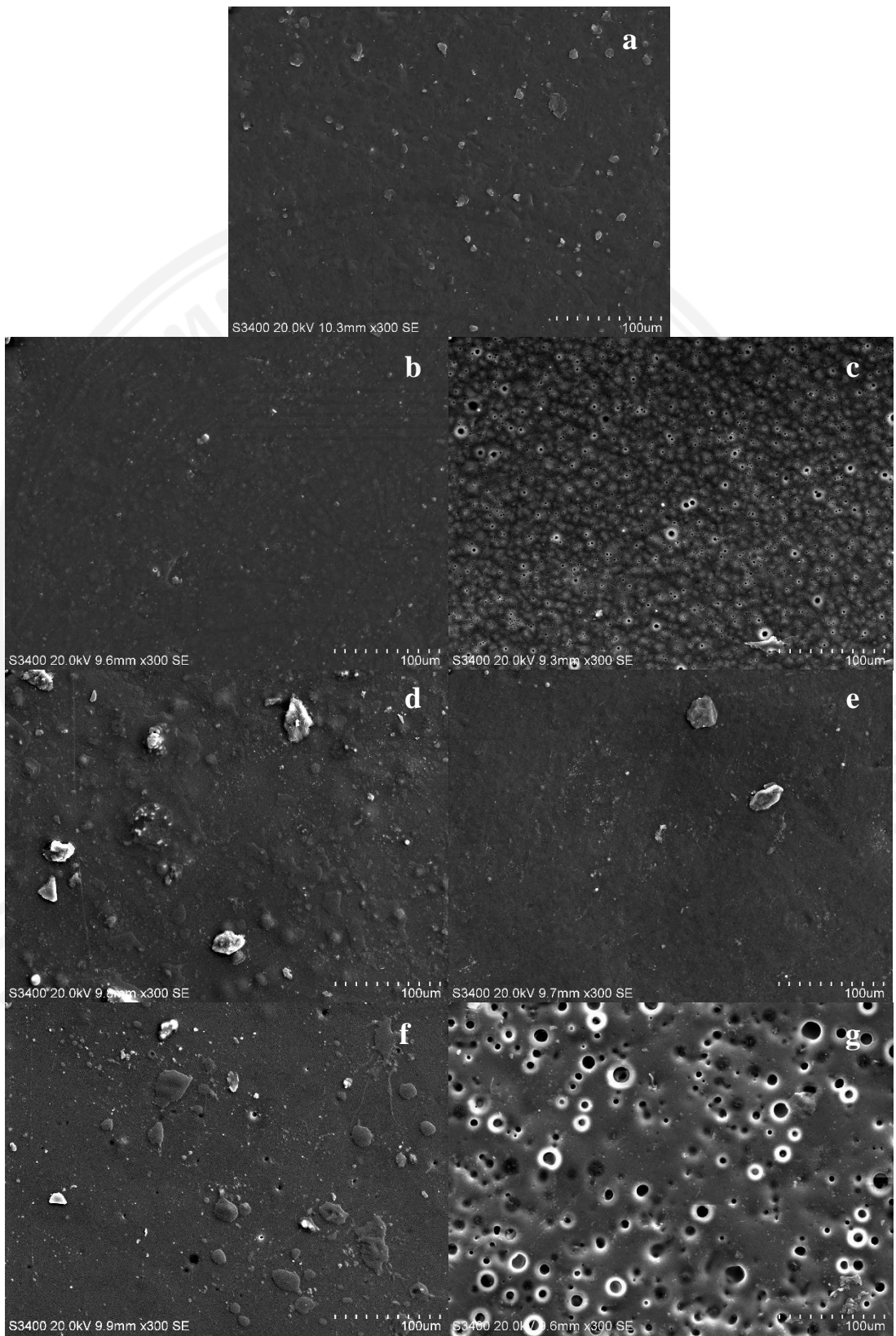
Figure 25 SEM images of surface of neat PLA(a), transparent zone of 0.2CNC-PVA(b), 0.2CNC(d), 0.5CNC(f), and opaque zone of 0.2CNC-PVA(c), 0.2CNC(e), 0.5CNC(g) films

4.2.6 Contact angle and surface wetting properties

Contact angle data is used to identify surface wetting properties of neat PLA and composite films. From Figure 27, neat PLA film has the contact angle value of about 74.9°, reflecting its hydrophobic nature or low surface wetting behaviors. When CNC was added into PLA, the contact angle of films decreased because CNC contain a lot of –OH functional groups which can increase the hydrophylicity of composite films. The contact angle of 0.2CNC and 0.5CNC decrease about 11-15%. This indicates that wetting of surface is more favorable, and the fluid spread over a large surface area. This is because there is CNC migrates on the surface of composite films, refered to SEM images. However, when PVA surfactant was added in 0.2CNC-PVA, CNC migration is inside the PLA matrix. Therefore, the hydrophobic property is more favorable, and cause the increase of contact angle, compared to neat PLA film.

The contact angle is measured both transparent and opaque zones. The results indicate that the opaque zones 0.2CNC and 0.5CNC have much higher contact angle than transparent zones. It is because more porous that made more rough surface as shown in SEM images and cause more surface tension through the films. Nonetheless, 0.2CNC-PVA has nearly the same results of transparent and opaque zones.

Figure 26 Contact angle properties of neat PLA and composite films
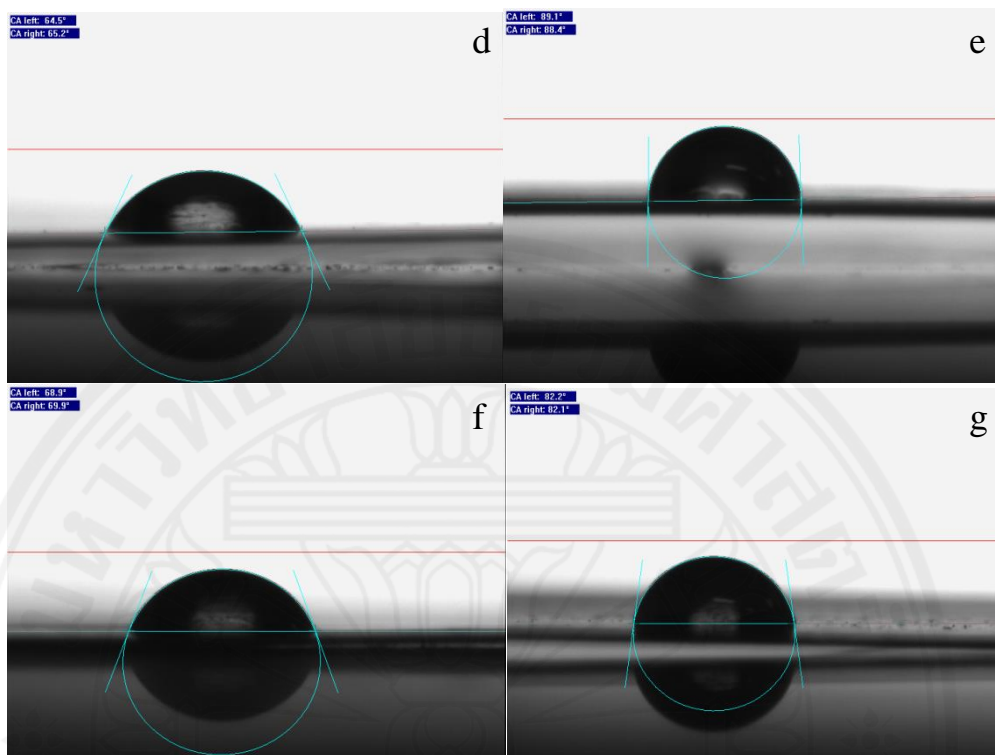
Figure 27 Contact angle images of neat PLA(a), transparent zone of 0.2CNC-
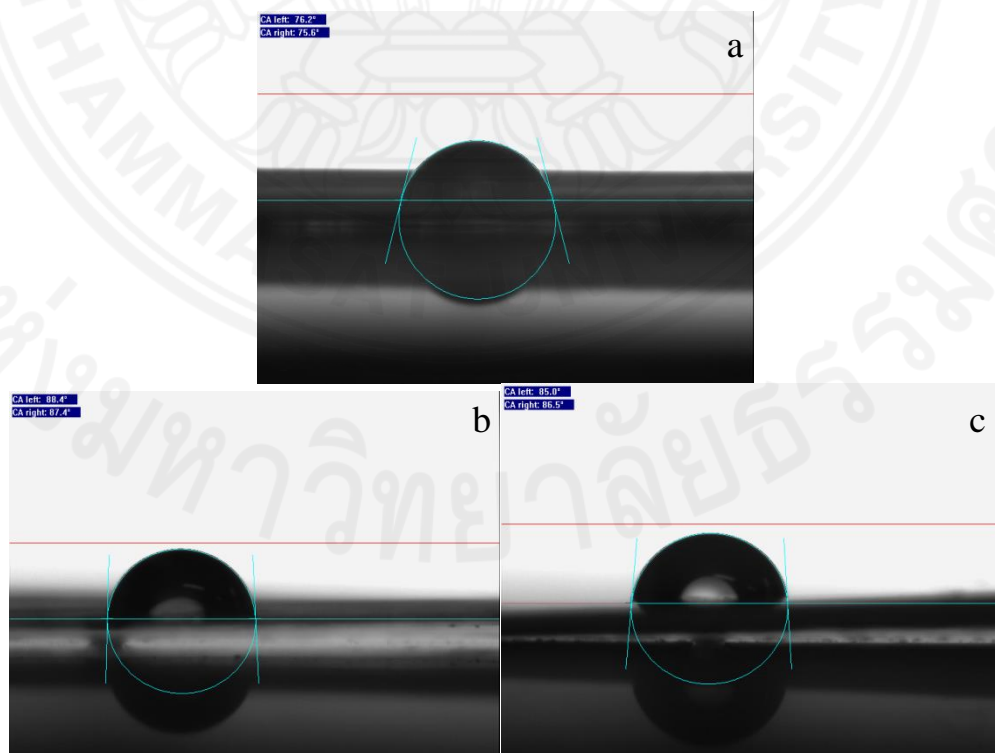PVA(b), 0.2CNC(d), 0.5CNC(f), and opaque zone of 0.2CNC-PVA(c), 0.2CNC(e),
0.5CNC(g)

4.2.7 Water vapour and gas permeability measurement

Table 9 Water vapor and gas permeability of films

Films	WVP (mm-cc/m²-day)	O₂ (mm-cc/m²-day)
Neat PLA	6.62 ± 0.44	61.78
0.2CNC-PVA	3.92 ± 1.43	
0.2CNC	4.33 ± 2.82	
0.5CNC	3.13 ± 1.65	72.40

The results of water vapour permeability (WVP) of neat PLA and
nanocomposite films are shown in Table 9. As the results, nanocomposite
films have lower WVP than neat PLA. WVP of 0.2CNC-PVA and 0.5CNC
are about 40% and 52% reduction from neat PLA, respectively, while WVP of
0.2CNC reduces about 35%. It is because of dense network that formed by

CNC, which have very small and uniform dimensions. Therefore, the complex dense network of nanofibers in PLA matrix can increase the tortuous pathway of molecules, which can limit diffusing molecules through composites. Thus, the barrier properties of composite films increase. The oxygen permeability of 0.5CNC was also measured, and it slightly increases. It might because of a very amount of CNC added into PLA, which cannot form more dense structures for oxygen barrier properties (Duan et al., 2013; S. S. Nair et al., 2014; Sanchez-Garcia et al., 2008; Song et al., 2014; Zenkiewicz & Richert, 2008).

Chapter 5

Conclusions and Recommendations

5.1 Research conclusions

Rice bran waste (RBW) was used as a raw material to prepare cellulose (RBC) by alkali and bleaching treatments. This cellulose samples were further used to prepare cellulose nanocrystals (CNC) by acid hydrolysis, in which some heterogeneous structured compounds are hydrolyzed as smaller molecules and precipitate, as called as PREP. The resulting CNC is used as reinforcing agent for polylactic acid (PLA) bioplastics by preparing as CNC/PLA composite films. Effect of the CNC composition in the composites was examined by varying the content from 0.2 to 0.5 wt%. An addition of surfactant in the preparation of the composites leads to a higher degree of dispersion of the CNC in the PLA matrix, resulting in further improvements in certain properties. This research can be concluded as follows:

5.1.1 Characterization of cellulose nanocrystals

After each specific treatment processes, rice bran waste (RBW), rice bran cellulose (RBC), cellulose nanocrystals (CNC), and the precipitate of cellulose nanocrystals (PREP) products showed different characteristics and properties. CNC and PREP had high values of crystallinity index, followed by RBC and RBW, respectively, as observed from XRD results. This is due to the acid hydrolysis, which removed the amorphous regions from the samples. The remaining samples contain higher crystalline content, leading to improvements in their thermal stability. TGA thremograms show that CNC and PREP had higher ash content than other samples, because residue sulfate groups from the reagent act like a flame retardant that can perform better thermal stability. The differences in terms of chemical structures, such as the presence of sulfate groups, are apparent in FTIR spectra. The morphology from SEM and TEM of each material was different because of chemical treatments. CNC had smaller diameter with more uniform size than others, which is a good property for reinforcing materials.

5.1.2 Characterization of neat PLA and nanocomposite films

The composite films were prepared by a solution cast method by using dichloromethane as a solvent. These composites were characterized and compared with neat PLA film. The results show that nanocomposite films had better mechanical properties, especially with 0.2CNC-PVA. This is because of its higher crystallinity, as clearly observed in XRD, DSC, and FTIR results. This leads to improvements in tensile strength and Young's modulus of the PLA matrix. Also, the higher crystallinity in nanocomposite films resulted in better thermal stability, as shown by a slight increase of degradation temperature in TGA thermograms. The presence of these CNC fibers is confirmed by SEM images. These nanocomposites exhibit higher hydrophilicity, as reflected by the lower contact angle values, due to the presence of more –OH groups from CNC fibers. However, they had lower water vapour permeability because CNC can increase a tortuous pathway and increase the barrier properties of PLA.

5.2 Recommendations

To obtain insight into characteristics and properties of the CNC/PLA composites materials, the following further work may be conducted:

5.2.1 Since CNC are not well dispersed in PLA solution, a process to disperse CNC in an organic phase similar to that of PLA, may be developed.

5.2.2 In this heterogeneous composite preparation process, the amount of water medium in CNC solution should be reduced as much as possible to avoid the presence of pore in the film samples and make better dispersion.

5.2.3 Dried CNC should be used instead of CNC that is dispersed water solution if it is possible.

References

Albalasmeh, A. A., & Ghezzehei, A. A. B. T. A. (2013). A new method for rapid determination of carbohydrate and totalcarbon concentrations using UV spectrophotometry. *Carbohydrate Polymers, 97*, 253-261.

Alemdar, A., & Sain, M. (2008). Isolation and characterization of nanofibers from agricultural residues – Wheat straw and soy hulls. *Bioresource Technology, 99*, 1664-1671.

Auras, R. A., Lim, L.-T., Selke, S. E. M., & Tsuji, H. (2010). *Poly(lactic acid): Synthesis, Structures, Properties, Processing, and Applications*. Canada: John Wiley & Sons.

Awal, A., Rana, M., & Sain, M. (2015). Thermorheological and mechanical properties of cellulose reinforced PLA bio-composites. *Mechanics of Materials, 80*, 87-95.

Burhenne, L., Messmer, J., Aicher, T., & Laborie, M.-P. (2013). The effect of the biomass components lignin, cellulose and hemicellulose on TGA and fixed bed pyrolysis. *Journal of Analytical and Applied Pyrolysis, 101*(0), 177-184. doi: http://dx.doi.org/10.1016/j.jaap.2013.01.012

Chandra, R., & Rustgi, R. (1998). Biodegradable polymers. *Progress in Polymer Science, 23*, 1273-1335.

Chang, S.-H., Lin, H.-T. V., Wu, G.-J., & Tsai, G. J. (2015). pH Effects on solubility, zeta potential, and correlation between antibacterial activity and molecular weight of chitosan. *Carbohydrate Polymers, 134*, 74-81.

Chen, Y., Liu, C., Chang, P. R., Cao, X., & Anderson, D. P. (2009). Bionanocomposites based on pea starch and cellulose nanowhiskers hydrolyzed from pea hull fibre: Effect of hydrolysis time. *Carbohydrate Polymers, 76*, 607-615.

Ciolacu, D., Ciolacu, F., & Popa, V. I. (2010). Amorphous cellulose - structure and characterization. *Cellulose Chemistry and Technology, 45*(1-2), 13-21.

Collard, F.-X., & Blin, J. (2014). A reviewonpyrolysisofbiomassconstituents:Mechanismsand composition of the products obtained from the conversion of cellulose, hemicelluloses and lignin. *Renewable and Sustainable Energy Reviews, 38*, 594-608.

Dash, R., Foston, M., & Ragauskas, A. J. (2013). Improving the mechanical and thermal properties of gelatin hydrogels cross-linked by cellulose nanowhiskers. *Carbohydrate Polymers, 91*, 638-645.

Deepa, B., Abraham, E., Cherian, B. M., Bismarck, A., Blaker, J. J., Pothan, L. A., . . . Kottaisamy, M. (2011). Structure, morphology and thermal characteristics of banana nano fibers obtained by steam explosion. *Bioresource Technology, 102*, 1988-1997.

Duan, Z., Thomas, N. L., & Huang, W. (2013). Water vapour permeability of poly(lactic acid) nanocomposites. *Journal of Membrane Science, 445*, 112-118.

Ehrenstein, G. W., Riedel, G., & Trawiel, P. (2004). *Thermal Analysis of Plastics*. Germany: Carl Hanser Verlag.

Elleuch, M., Bedigian, D., Roiseux, O., Besbes, S., Blecker, C., & Attia, H. (2011). Dietary fibre and fibre-rich by-products of food processing: Characterisation,

technological functionality and commercial applications: A review. *Food Chemistry, 124*, 411-421.

Esler, A., Edward, G., Angelo, G. J., James, S., & Henry, V. (1952). United States Patent No. US2727914 A.

Fakirov, S., & Bhattacharyya, D. (2007). *Handbook of Engineering Biopolymers: Homopolymers, Blends, and Composites*. Germany: Hanser Gardner Publication.

Ford, E. N. J., Mendon, S. K., Thames, S. F., & Rawlins, J. W. (2010). X-ray diffraction of cotton treated with neutralized vegetable oil-based macromolecular crosslinkers. *Journal of Engineered Fibers and Fabrics, 5*(1), 10-20.

Garlotta, D. (2001). A Literature Review of Poly(Lactic Acid). *Journal of Polymers and the Environment, 9*(2), 63-84.

Gonzalez, J. S., Ludueña, L. N., Ponce, A., & Alvarez, V. A. (2014). Poly(vinyl alcohol)/cellulose nanowhiskers nanocomposite hydrogels for potential wound dressings. *Materials Science and Engineering C, 34*, 54-61.

Gu, J., Catchmarka, J. M., Kaiser, E. Q., & Archibald, D. D. (2013). Quantification of cellulose nanowhiskers sulfate esterification levels. *Carbohydrate Polymers 92 (2013) 1809– 1816, 92*, 1809-1816.

Guo, J., & Catchmark, J. M. (2012). Surface area and porosity of acid hydrolyzed cellulose nanowhiskers and cellulose produced by Gluconacetobacter xylinus. *Carbohydrate Polymers, 87*, 1026-1037.

Haafiz, M. K. M., Hassan, A., Zakaria, Z., & Inuwa, I. M. (2014). Isolation and characterization of cellulose nanowhiskers from oilpalm biomass microcrystalline cellulose. *Carbohydrate Polymers, 103*, 119-125.

Ház, A., Jablonský, M., Orságová, A., & Šurina, I. (2013). *Determination of temperature regions in thermal degradation of lignin*. Paper presented at the Renewable Energy Sources, High Tatras, Slovak Republic.

Hebeish, A., Farag, S., Sharaf, S., & Shaheen, T. I. (2014). Thermal responsive hydrogels based on semi interpenetratingnetwork of poly(NIPAm) and cellulose nanowhiskers. *Carbohydrate Polymers, 102*, 159-166.

Hossain, K. M. Z., Ahmed, I., Parsons, A. J., Scotchford, C. A., Walker, G. S., Thielemans, W., & Rudd, C. D. (2012). Physico-chemical and mechanical properties of nanocomposites prepared using cellulose nanowhiskers and poly(lactic acid). *Journal of Materials Science, 47*, 2675-2686.

Jhawer, M., & Vakil, D. E. Rice Bran Oil - "The Age Old Health Oil". from http://www.medindia.net/patients/lifestyleandwellness/rice-bran-oil-benefits.htm

Jin, W., Singh, K., & Zondlo, J. (2013). Pyrolysis kinetics of physical components of wood and wood-polymers using Isoconversion method. *Agriculture, 3*, 12-32.

Johar, N., Ahmad, I., & Dufresnec, A. (2012). Extraction, preparation and characterization of cellulose fibres and nanocrystals from rice husk. *Industrial Crops and Products, 37*, 93-99.

Jonoobi, M., Khazaeian, A., Tahir, P. M., Azry, S. S., & Oksman, K. (2011). Characteristics of cellulose nanofibers isolated from rubberwood and empty fruit bunches of oil palm using chemo-mechanical process. *Cellulose, 18*, 1085-1095.

Kalia, S., Kaith, B. S., & Kaur, I. (2011). *Cellulose Fibers: Bio- and Nano-Polymer Composites*. Germany: Springer.

Kim, D.-Y., Nishiyama, Y., Wada, M., & Kuga, S. (2001). High-yield carbonization of cellulose by sulfuric acid impregnation. *Cellulose, 8*, 29-33.

Kong, F., Parhiala, K., Wang, S., & Fatehi, P. (2015). Preparation of cationic softwood kraft lignin and its application in dye removal. *European Polymer Journal, 67*(0), 335-345. doi: http://dx.doi.org/10.1016/j.eurpolymj.2015.04.004

Kržan, A. (2012). Biodegradable polymers and plastics. from www.plastice.org

LaCourse, N. L., Chicalo, K., Zallie, J. P., & Altieri, P. A. (1994). United State Patent No.

Lee, J. H., Park, S. H., & Kim, a. S. H. (2013). Preparation of cellulose nanowhiskers and their reinforcing effect in polylactide. *Macromolecular Research, 21*(11), 1218-1225.

Li, R., Fei, J., Cai, Y., Li, Y., Feng, J., & Yao, J. (2009). Cellulose whiskers extracted from mulberry: A novel biomass production. *Carbohydrate Polymers, 76*, 94-99.

Lu, H., Gui, Y., Zheng, L., & Liu, X. (2013). Morphological, crystalline, thermal and physicochemical properties of cellulose nanocrystals obtained from sweet potato residue. *Food Research International, 50*, 121-128.

Lu, P., & Hsieh, Y.-L. (2012a). Cellulose isolation and core–shell nanostructures of cellulose nanocrystals from chardonnay grape skins. *Carbohydrate Polymers, 87*, 2546-2553.

Lu, P., & Hsieh, Y.-L. (2012b). Preparation and characterization of cellulose nanocrystals from rice straw. *Carbohydrate Polymers, 87*, 564-573.

Maheswari, C. U., Reddy, K. O., Muzenda, E., Guduri, B. R., & Rajulu, A. V. (2012). Extraction and characterization of cellulose microfibrils from agricultural residue - Cocos nucifera L. *BIomass and bioenergy, 46*, 555-563.

Maniaw, P. (2009). *Study on Effect of cellulose microfibrils on properties of biopolymer films.* (Master of Engineering), King Mongkut's University of Technology Thonburi, Thailand.

McKEE, L. H., & LATNER, T. A. (2000). Underutilized sources of dietary fiber: A review. *Plant Foods for Human Nutrition, 55*, 285-304.

Moran-Mirabal, J. M. (2013). *Advanced-Microscopy Techniques for the Characterization of Cellulose Structure and Cellulose-Cellulase Interactions*.

Mudgil, D., & Barak, S. (2013). Composition, properties and health benefits of indigestible carbohydrate polymers as dietary fiber: A review. *International Journal of Biological Macromolecules, 61*, 1-6.

Nair, L. S., & Laurencin, C. T. (2007). Biodegradable polymers as biomaterials. *Progress in Polymer Science, 32*, 762-798.

Nair, S. S., Zhu, J., Deng, Y., & Ragauskas, A. J. (2014). High performance green barriers based on nanocellulose. *Sustainable Chemical Processes, 2*(23), 1-7. Retrieved from http://www.sustainablechemicalprocesses.com/content/2/1/23 website:

Neto, W. P. F., Silvério, H. A., Dantas, N. O., & Pasquini, D. (2013). Extraction and characterization of cellulose nanocrystals from agro-industrial residue – Soy hulls. *Industrial Crops and Products, 42*, 480-488.

Norgren, M., & Edlund, H. (2014). Lignin: Recent advances and emerging applications. *Current Opinion in Colloid & Interface Science, 19*(5), 409-416. doi: http://dx.doi.org/10.1016/j.cocis.2014.08.004

Pasquini, D., Teixeira, E. d. M., Curvelo, A. A. d. S., Belgacemc, M. N., & Alain Dufresnea. (2010). Extraction of cellulose whiskers from cassava bagasse and their applications as reinforcing agent in natural rubber. *Industrial Crops and Products, 32*, 486-490.

Paula, E. L. d., Mano, V., & Pereira, F. V. (2011). Influence of cellulose nanowhiskers on the hydrolytic degradation behavior of poly(D,L-lactide). *Polymer Degradation and Stability, 96*, 1631-1638.

Petersson, L., Kvien, I., & Oksman, K. (2007). Structure and thermal properties of poly(lactic acid)/cellulose whiskers nanocomposite materials. *Composites Science and Technology, 67*, 2535-2544.

Pornchalermpong, P., & Rattanapanon, N. Rice. from http://www.foodnetworksolution.com/wiki/word/1657/rice%E0%B8%82%E0%B9%89%E0%B8%B2%E0%B8%A7

Rahamim, J. (2013). Electrostatic Force Microscopy of Electrospun Polymer Nanofibers with Embedded Carbon Nanotubes.

Randriamanantena, T., Razafindramisa, F. L., Ramanantsizehena, G., Bernes, A., & Lacabane, C. *Thermal behaviour of three woods of Madagascar by thermogravimetric analysis in inert atmosphere*. Université Paul Sabatier Toulouse III.

Raquez, J.-M., Murena, Y., Goffin, A.-L., Habibi, Y., Ruelle, B., DeBuyl, F., & Dubois, P. (2012). Surface-modification of cellulose nanowhiskers and their use as nanoreinforcers into polylactide: A sustainably-integrated approach. *Composites Science and Technology, 72*, 544-549.

Rodriguez, N. L. G. d., Thielemans, W., & Dufresne, A. (2006). Sisal cellulose whiskers reinforced polyvinyl acetate nanocomposites. *Cellulose, 13*, 261-270.

Rosa, M. F., Medeiros, E. S., Malmonge, J. A., Gregorski, K. S., Wood, D. F., Mattoso, L. H. C., . . . Imam, S. H. (2010). Cellulose nanowhiskers from coconut husk fibers: Effect of preparation conditions on their thermal and morphological behavior. *Carbohydrate Polymers, 81*, 83-92.

Rotliwala, Y. C., & Parikh, P. A. (2011). Thermal degradation of rice-bran with high density polyethylene: A kinetic study. *Korean Journal of Chemical Engineering, 28*(3), 788-792.

Sanchez-Garcia, M. D., Gimenez, E., & Lagaron, J. M. (2008). Morphology and barrier properties of solvent cast composites of thermoplastic biopolymers and purified cellulose fibers. *Carbohydrate Polymers, 71*, 235-244.

Shah, N., Ul-Islam, M., Khattak, W. A., & Park, J. K. (2013). Overview of bacterial cellulose composites: A multipurpose advanced material. *Carbohydrate Polymers, 98*(2), 1585-1598. doi: http://dx.doi.org/10.1016/j.carbpol.2013.08.018

Silvério, H. A., Netoa, W. P. F., Dantasb, N. O., & Pasquini, D. (2013). Extraction and characterization of cellulose nanocrystals from corncob for application as reinforcing agent in nanocomposites. *Industrial Crops and Products, 44*, 427-436.

Song, Z., Xiao, H., & Zhao, Y. (2014). Hydrophobic-modified nano-cellulose fiber/PLA biodegradable composites for lowering water vapor transmission rate (WVTR) of paper. *Carbohydrate Polymers, 111*, 442-448.

Spagnol, C., Rodrigues, F. H. A., Neto, A. G. V. C., Pereira, A. G. B., Fajardo, A. R., Radovanovic, E., . . . Muniz, E. C. (2012). Nanocomposites based on poly(acrylamide-co-acrylate) and cellulose nanowhiskers. *European Polymer Journal, 48*, 454-463.

Tehrani, A. D., & Neysi, E. (2013). Surface modification of cellulose nanowhisker throughout graft polymerization of 2-ethyl-2-oxazoline. *Carbohydrate Polymers, 97*, 98-104.

Teixeira, E. d. M., Bondancia, T. J., Teodoro, K. B. R., Corrêa, A. C., Marconcini, J. M., & Mattoso, L. H. C. (2011). Sugarcane bagasse whiskers: Extraction and characterizations. *Industrial Crops and Products, 33*, 63-66.

Trachea, D., Donnotb, A., Khimechea, K., Benelmirb, R., & Brosse, N. (2014). Physico-chemical properties and thermal stability of microcrystallinecellulose isolated from Alfa fibres. *Carbohydrate Polymers, 104*, 223-230.

Visakh, P. M., Thomas, S., Oksman, K., & Mathew, A. P. (2012). Crosslinked natural rubber nanocomposites reinforced with cellulose whiskers isolated from bamboo waste: Processing and mechanical/thermal properties. *Composites: Part A, 43*, 735-741.

Wang, N., Ding, E., & Cheng, R. (2007). Thermal degradation behaviors of spherical cellulose nanocrystals with sulfate groups. *Polymer, 48*, 3486-3493.

Wanrosli, W. D., Rohaizu, R., & Ghazali, A. (2011). Synthesis and characterization of cellulose phosphate from oil palm empty fruit bunches microcrystalline cellulose. *Carbohydrate Polymers, 84*, 262-267.

Zenkiewicz, M., & Richert, J. (2008). Permeability of polylactide nanocomposite films for water vapour, oxygen and carbon dioxide. *Polymer Testing, 27*, 835-840.

Appendices

Appendix A

Proximate analysis of rice bran waste

ที่ ศธ 0513.12201/580737

สถาบันค้นคว้าและพัฒนาผลิตภัณฑ์อาหาร
มหาวิทยาลัยเกษตรศาสตร์
50 งามวงศ์วาน จตุจักร กรุงเทพฯ 10900
โทรศัพท์ 0 2942 8629-35
โทรสาร 0 2942 7601

รายงานผลการทดสอบ

คำขอบริการเลขที่	:	580737	วันที่	8 มกราคม 2558	
ผู้ขอรับบริการ	:	โครงการวิจัยและพัฒนาภาครัฐร่วมเอกชนในเชิงพาณิชย์			
		เลขที่ 123 หมู่ที่ 16 ถนนมิตรภาพ ตำบลในเมือง			
		อำเภอเมือง จังหวัดขอนแก่น 40002			
ชื่อตัวอย่าง	:	กากรำข้าวสกัด			
ชนิดตัวอย่าง	:	-			
ภาชนะบรรจุ	:	ถุงพลาสติกปิดสนิท			
ขนาดบรรจุต่อหน่วย	:	600 กรัม			
ลักษณะตัวอย่าง	:	ผงละเอียดสีน้ำตาลอ่อน			
วันที่รับตัวอย่าง	:	20 พฤศจิกายน 2557			
วันที่ทำการทดสอบ	:	28 พฤศจิกายน – 25 ธันวาคม 2557			

รายการทดสอบ	ผลการทดสอบ	วิธีทดสอบ	หมายเหตุ
Moisture, %	9.06	In house method based on AOAC (2012) 925.45	-
Protein, % (factor 6.25)	12.47	In house method based on AOAC (2012) 991.20	-
Fat, %	1.35	In house method based on AOAC (2012) 989.05	-
Ash, %	7.80	In house method based on AOAC (2012) 938.08	-
Total Carbohydrate, % (by difference ; include crude fiber)	69.32	In house method based on AOAC (2005) by Calculation	-
Total Calories, Kcal/100 g	339.31	In house method based on AOAC (2005) by Calculation	-
Calories from fat, Kcal/100 g	12.15	In house method based on AOAC (2005) by Calculation	-
Dietary fiber, %	27.14	In house method based on AOAC (2012) 985.29	-

ผู้รายงาน

ลงชื่อ..
(นางสาวศุภธิดา พิมพิสณฑ์)
นักวิทยาศาสตร์

ผู้รับรอง

ลงชื่อ..
(นางจันทร์สุดา จริยวัฒนวิจิตร)
หัวหน้าศูนย์บริการประกันคุณภาพอาหาร

ลงชื่อ..
(นางพัชรี ฟุ้งตระกูล)
ผู้อำนวยการ

รายงานผลการวิเคราะห์นี้รับรองเฉพาะตัวอย่างที่ได้รับเท่านั้น และห้ามนำไปใช้ประโยชน์ในการโฆษณา
เอกสารทุกฉบับต้องมีตราประทับของสถาบันฯ และลงนามกำกับโดยผู้มีอำนาจ
ศูนย์บริการประกันคุณภาพอาหาร โทร. 02 942 8629-35 ต่อ 800, 811 โทรสาร 02 9427601-2

Figure A-1 Proximate analysis results of rice bran waste

Appendix B

Percentage of cellulose, hemicellulose, and lignin contents

Table B-1 Titration volume of rice bran waste (RBW) and rice bran cellulose (RBC)

No.	Blank (mL)	Cellulose		Lignin	
		V_1 (mL)	V_2 (mL)	V_1 (mL)	V_2 (mL)
1	47.0	26.9	31.5	39.0	41.0
2	47.1	27.2	33.9	38.1	42.5
3	47.7	31.0	33.7	38.3	42.5
Average	47.27	28.37	33.03	38.47	42.00

Where: V_1 = titration volume of rice bran waste (RBW)

V_2 = titration volume of rice bran cellulose (RBC)

Percentage of cellulose calculation

Rice bran waste

% Cellulose = 100 - [6.85 (V_2 - V_1) $\times$ N $\times$ 20 / (A $\times$ W)]

= 100 - [6.85 (47.27 - 28.37) $\times$ 0.1 $\times$ 20 / (10 $\times$ 1.5)]

= 82.8

Rice bran cellulose

% Cellulose = 100 - [6.85 (V_2 - V_1) $\times$ N $\times$ 20 / (A $\times$ W)]

= 100 - [6.85 (47.27 - 33.03) $\times$ 0.1 $\times$ 20 / (10 $\times$ 1.5)]

= 87.0

Where: V_1 = Titration of sample

V_2 = Blank titration

N = Exact normality of the ferrous ammonium sulfate solution

A = volume of the filtrate used, mL

W = Weight of sample

Percentage of lignin calculation

Rice bran waste

% Lignin = 6.85 (V_2 - V_1) × N × 20 / (A × W)

   = 6.85 (47.27 - 38.47) × 0.1 × 20 / (10 × 1.5)]

          = 8.0

Rice bran cellulose

% Lignin = 6.85 (V_2 - V_1) × N × 20 / (A × W)

          = 6.85 (47.27 - 42.00) × 0.1 × 20 / (10 × 1.5)

          = 4.8

Percentage of hemicellulose calculation

Rice bran waste

     % Hemicellulose = 100 - (% Cellulose - % Lignin)

                = 100 – (82.8 – 8.0)

                = 9.2

Rice bran cellulose

% Hemicellulose = 100 - (% Cellulose - % Lignin)

            = 100 – (87.0 – 4.8)

            = 8.2

Appendix C

Yield percent of products

Yield percent of RBC from RBW calculation

$$\% \text{ Yield} = \frac{\text{Weight of products}}{\text{Weight of raw mateirals}} \times 100$$

$$= \frac{26.65 \text{ g}}{540 \text{ g}} \times 100$$

$$= 4.9$$

Yield percent of CNC from RBC calculation

$$\% \text{ Yield} = \frac{86.4 \times 10^{-3} \text{ g}}{3 \text{ g}} \times 100$$

$$= 2.9$$

Yield percent of CNC from RBW calculation

$$\% \text{ Yield} = \frac{86.4 \times 10^{-3} \text{ g}}{60.8 \text{ g}} \times 100$$

$$= 0.1$$

Appendix D

Concentration of cellulose nanocrystals solution

Standard curve calculation

<u>Glucose dilution (0-100 µg/mL)</u>

20 µg/mL: $C_1V_1 = C_2V_2$

  (20 µg/mL)(5 mL) = (1000 µg/mL)V_2

  $V_2 = 0.1$ mL

40 µg/mL: $C_1V_1 = C_2V_2$

  (40 µg/mL)(5 mL) = (1000 µg/mL)V_2

  $V_2 = 0.2$ mL

60 µg/mL: $C_1V_1 = C_2V_2$

  (60 µg/mL)(5 mL) = (1000 µg/mL)V_2

  $V_2 = 0.3$ mL

80 µg/mL: $C_1V_1 = C_2V_2$

  (80 µg/mL)(5 mL) = (1000 µg/mL)V_2

  $V_2 = 0.4$ mL

100 µg/mL: $C_1V_1 = C_2V_2$

  (100 µg/mL)(5 mL) = (1000 µg/mL)V_2

  $V_2 = 0.5$ mL

CNC dilution 100 times: Sample 40 µL in water 3960 µL

CNC concentration calculation

$$Y = 0.0102X + 0.0003$$

$$X = (Y - 0.0003)/0.0102$$

$$= (0.5687 - 0.0003)/0.0102$$

$$= 55.7255 \text{ µg/mL} \rightarrow \text{dilute 100 times}$$

Actual concentration   = 5572.55 µg/mL
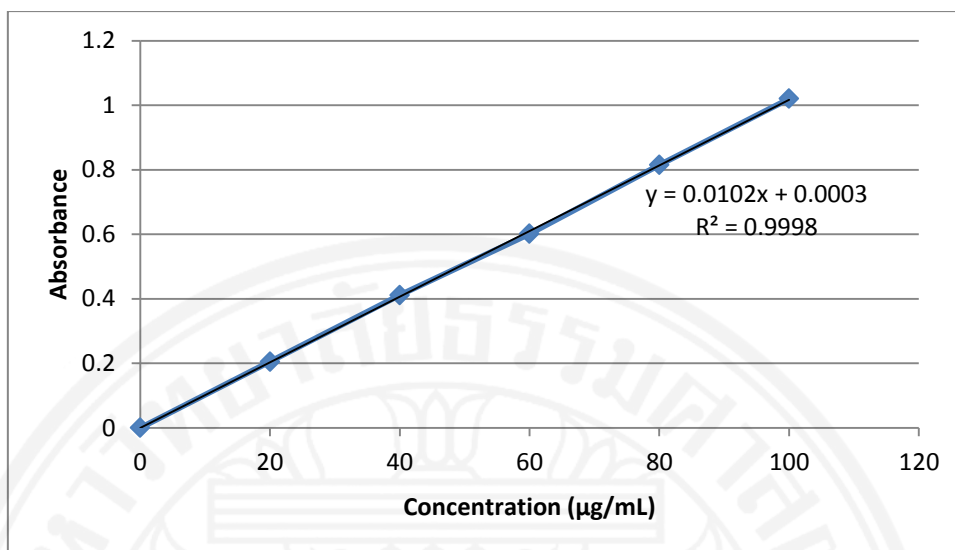
Figure D-1 Standard curve of glucose from UV-VIS spectroscopy at 315 nm

Table D-1 Raw data from UV-VIS spectroscopy

Concentration (μg/mL)	Absorbance at 315 nm
0	0
	-0.0067
	-0.0042
20	0.2002
	0.205
	0.2066
40	0.4117
	0.4453
	0.4428
60	0.6013
	0.7267
	0.6749
80	0.815
	0.9359
	0.8844
100	1.02
	1.1366
	1.0682
CNC	0.5687
	0.5638
	0.6524

Appendix E

Films calculation

PLA 4043D, density = 1.24 g/mL

Dichloromethane (DCM) = 1.33 g/mL

5% PLA/DCM calculation

Average density = (0.05)(Density of PLA) + (0.95)(Density of DCM)

$$= (0.05)(1.24 \text{ g/mL}) + (0.95)(1.33 \text{ g/mL})$$

$$= 1.3255 \text{ g/mL}$$

For 60 mL solution = 1.3255 g/mL × 60 mL = 79.53 g

The amount of PLA pellets = 0.05 × 79.53 = 3.98 g

The amount of DCM $\quad = 0.95 \times 79.53 = 75.55$ g

0.2 wt% CNC/PLA preparation

The amount of CNC = (0.2/100) × 3.98 g

$$= 7.96 \times 10^{-3} \text{ g}$$

$$= 7960 \text{ µg}$$

The volume of CNC $= \dfrac{7960 \text{ µg}}{5572.55 \text{ µg/mL}} = 1.43$ mL

The amount of PVA surfactant (1:10) $= \dfrac{7960 \text{ µg}}{10} = 796$ µg = 0.796 mg

0.5wt% CNC/PLA preparation

The amount of CNC = (0.5/100) × 3.98 g

$$= 1.99 \times 10^{-2} \text{ g}$$

$$= 19900 \text{ µg}$$

The volume of CNC $= \dfrac{19900 \text{ µg}}{5572.55 \text{ µg/mL}} = 3.57$ mL

Appendix F

Crystallinity Index from X-ray diffractograms

Crystallinity Index (Cr.I.) equation

$$\text{Cr.I. (\%)} = (S_c / S_t) \cdot 100$$

Where: S_c is area of the crystalline domain

S_t is area of the total domain

Rice bran waste (RBW)

Table F-1 XRD peak and area of RBW

Amorphous		Crystalline	
Peak (°)	Area	Peak (°)	Area
18.85	6795.51	15.07	598.67
19.66	26226.3		
22.12	4463.16		
31.58	3246.41		
Total	40731.38		598.67

$$\text{Cr.I. (\%)} = \frac{598.67}{40731.38 + 598.67} \times 100 = 1.4\ \%$$
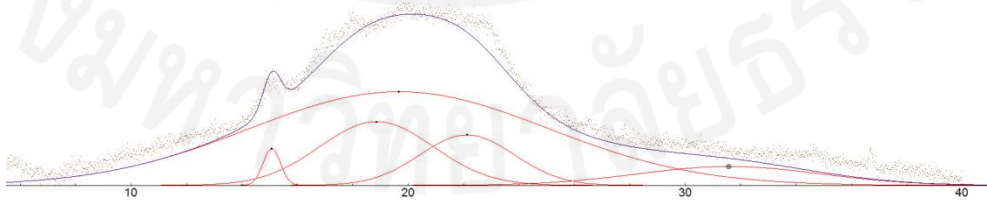
Figure F-1 X-ray diffractogram of rice bran waste (RBW)

70

Rice bran cellulose (RBC)

Table F-2 XRD peak and area of RBC

Amorphous		Crystalline	
Peak(°)	Area	Peak(°)	Area
11.89	1322.07	15.47	8463.36
18.44	19440.8	21.44	9922.96
22.14	5023.22	22.32	8168.08
28.5	2425.71	34.52	1001.45
34.75	3442.49		
Total	31654.29		27555.85

$$\text{Cr.I. } (\%) = \frac{27555.85}{27555.85 + 31654.29} \times 100 = 46.5\ \%$$
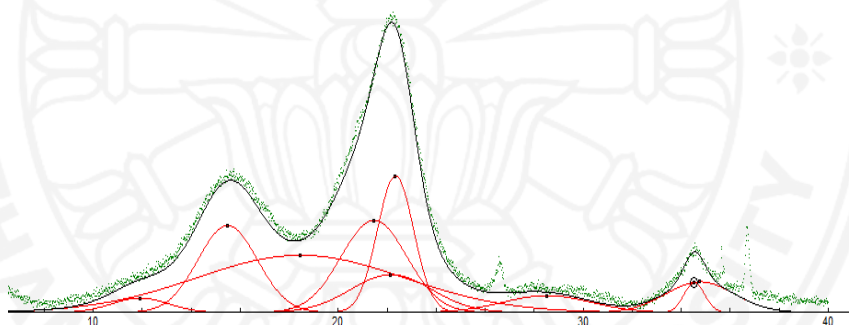
Figure F-2 X-ray diffractogram of rice bran cellulose (RBC)

Cellulose nanocrystals (CNC)

Table F-3 XRD peak and area of CNC

Amorphous		Crystalline	
Peak (°)	Area	Peak (°)	Area
20.04	1015.88	14.71	86.16
		20.88	302.67
		26.65	96.27
Total	1015.88		485.10

$$\text{Cr.I. } (\%) = \frac{485.10}{1015.88 + 485.10} \times 100 = 47.8\ \%$$

71
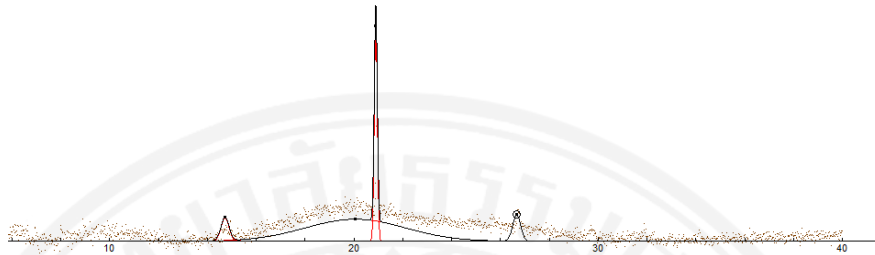
Figure F-3 X-ray diffractogram of cellulose nanocrystals (CNC)

<u>Precipitate of CNC (PREP)</u>

Table F-4 XRD peak and area of PREP

Amorphous		Crystalline	
Peak (°)	Area	Peak (°)	Area
20.03	219.37	20.89	524.91
22.66	830.28	21.5	130.40
		26.75	347.44
Total	1049.65		1002.75

$$Cr.I. \ (\%) = \frac{1002.75}{1002.75+1049.65} \times 100 = 48.9 \ \%$$
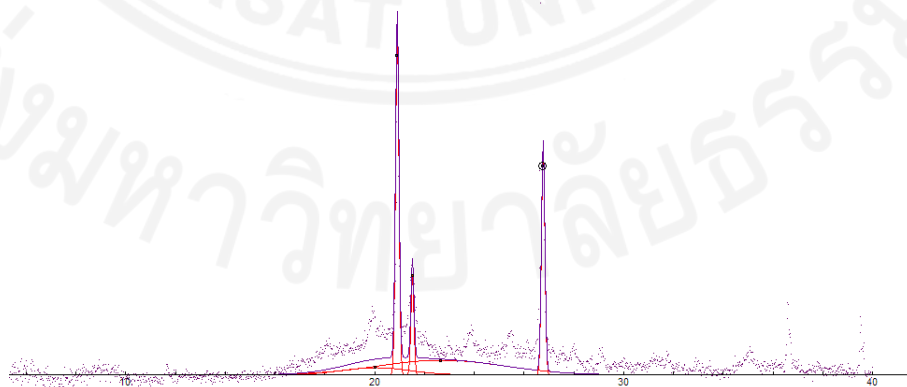
Figure F-4 X-ray diffractogram of cellulose nanocrystals precipitate (PREP)

Neat PLA film

Table F-5 XRD peak and area of neat PLA before mechanical testing

Amorphous		Crystalline	
Peak (°)	Area	Peak (°)	Area
10.33	15685.1	16.88	642.09
12.48	5058.35		
14.48	9492.7		
21.63	10188.9		
16.77	27361.1		
Total	67786.15		642.09

$$\text{Cr.I. }(\%) = \frac{642.09}{642.09 + 67786.15} \times 100 = 0.9\ \%$$
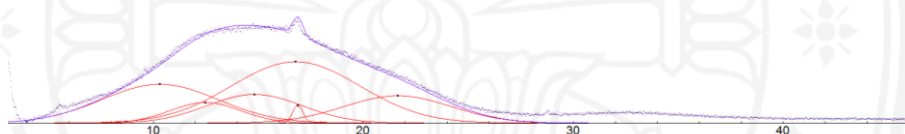
Figure F-5 X-ray diffractogram of neat PLA before mechanical testing

Table F-6 XRD peak and area of neat PLA after mechanical testing

Amorphous		Crystalline	
Peak (°)	Area	Peak (°)	Area
9.03	7436.79	16.83	444.95
12.17	6819.4		
16.03	4530.37		
20.28	19844.6		
Total	38631.16		444.95

$$\text{Cr.I. }(\%) = \frac{444.95}{444.95 + 38631.16} \times 100 = 1.1\ \%$$
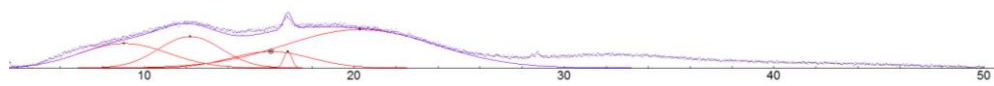
Figure F-6 X-ray diffractogram of neat PLA after mechanical testing

73

0.2CNC-PVA film

Table F-7 XRD peak and area of 0.2CNC-PVA before mechanical testing

Amorphous		Crystalline	
Peak (°)	Area	Peak (°)	Area
13.23	3884.67	15.11	228.86
17.34	11599.1	16.91	2540.67
		19.4	727.46
		22.63	398.54
Total	15483.77		3895.52

$$\text{Cr.I. (\%)} = \frac{3895.52}{3895.52+15483.77} \times 100 = 20.1\ \%$$
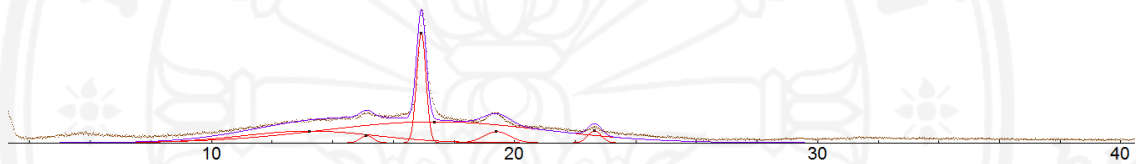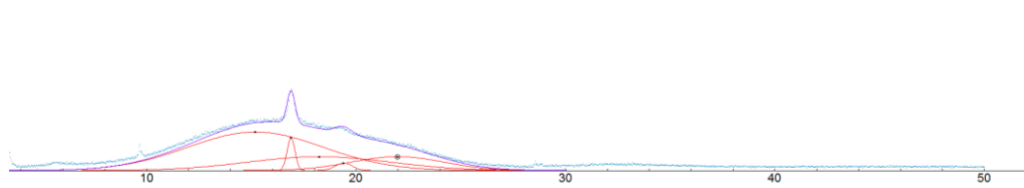

Figure F-7 X-ray diffractogram of 0.2CNC-PVA before mechanical testing

Table F-8 XRD peak and area of 0.2CNC-PVA after mechanical testing

Amorphous		Crystalline	
Peak (°)	Area	Peak (°)	Area
14.23	14817.4	16.81	282.3
17.72	8371.18		
21.81	7245.61		
Total	30434.19		282.3

$$\text{Cr.I. (\%)} = \frac{282.3}{232.3+30434.19} \times 100 = 0.9\ \%$$
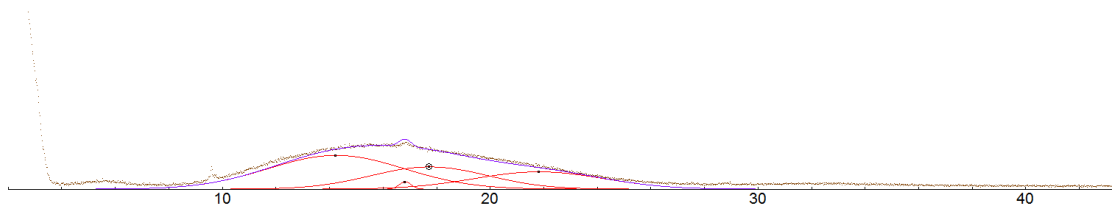
Figure F-8 X-ray diffractogram of 0.2CNC-PVA after mechanical testing

74

0.2CNC film

Table F-9 XRD peak and area of 0.2CNC before mechanical testing

Amorphous		Crystalline	
Peak (°)	Area	Peak (°)	Area
17.09	10271.3	15.04	210.76
		16.94	1673.13
		19.36	191.60
		22.56	242.70
Total	10271.3		2318.2

$$\text{Cr.I. (\%)} = \frac{2318.2}{2318.2 + 10271.3} \times 100 = 18.4 \ \%$$
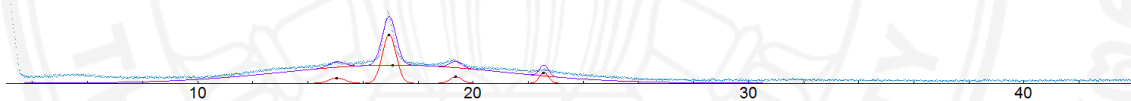
Figure F-9 X-ray diffractogram of 0.2CNC before mechanical testing

Table F-10 XRD peak and area of 0.2CNC after mechanical testing

| Amorphous		Crystalline	
Peak (°)	Area	Peak (°)	Area
15.18	22954.8	16.88	1128.76
18.22	8686.05	19.4	551.82
21.97	5645.93		
Total	37286.78		1680.58

$$\text{Cr.I. (\%)} = \frac{1680.58}{1680.58 + 37286.78} \times 100 = 4.3 \ \%$$

Figure F-10 X-ray diffractogram of 0.2CNC after mechanical testing

0.5CNC film

Table F-11 XRD peak and area of 0.5CNC before mechanical testing

Amorphous		Crystalline	
Peak (°)	Area	Peak (°)	Area
13.13	369.157	14.93	49.18
16.91	4931.89	16.95	1288.01
21.6	904.158	19.29	358.3
		22.53	81.75
Total	6205.21		1971.61

$$\text{Cr.I. (\%)} = \frac{1971.61}{1971.61+6205.21} \times 100 = 22.3 \text{ \%}$$
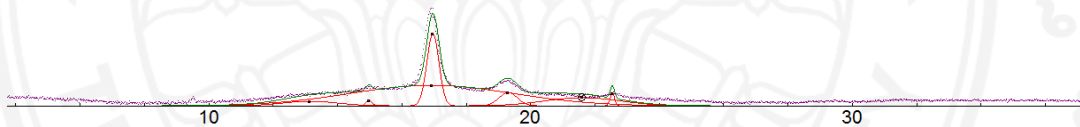
Figure F-11 X-ray diffractogram of 0.5CNC before mechanical testing

Table F-12 XRD peak and area of 0.5CNC after mechanical testing

Amorphous		Crystalline	
Peak (°)	Area	Peak (°)	Area
17.34	4995.12	16.72	587.59
13.96	1910.93		
21.61	3770.34		
Total	10676.39		587.59

$$\text{Cr.I. (\%)} = \frac{587.59}{587.59+10676.39} \times 100 = 5.2 \text{ \%}$$

76
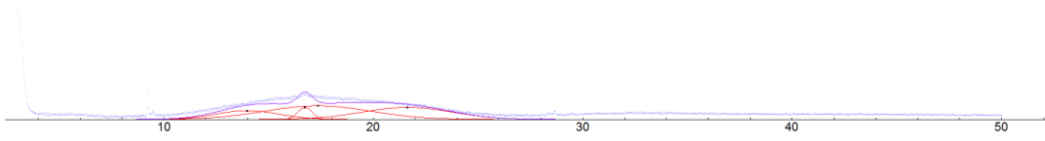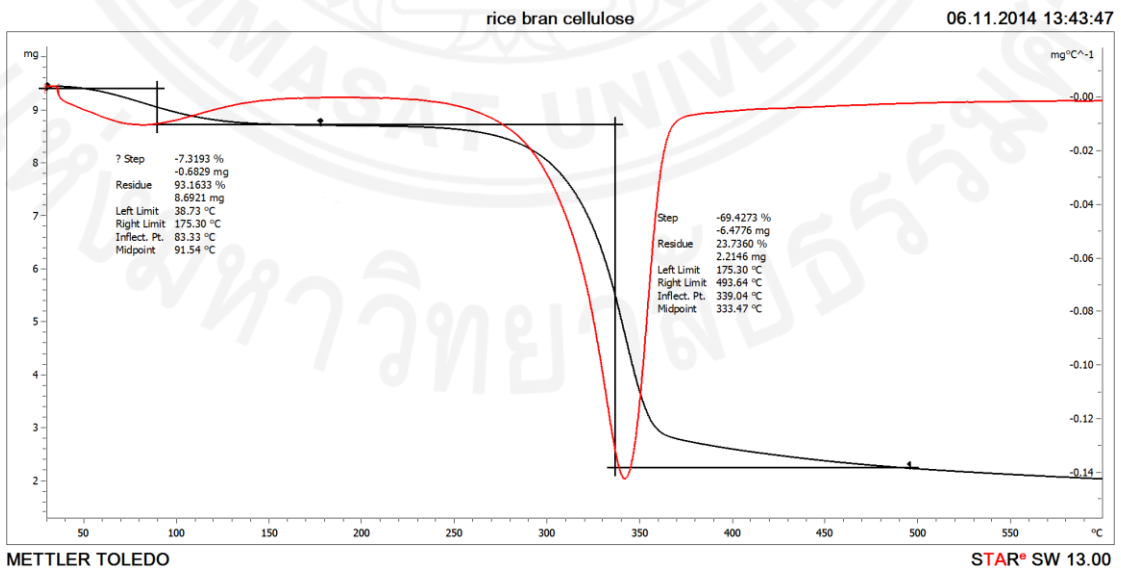
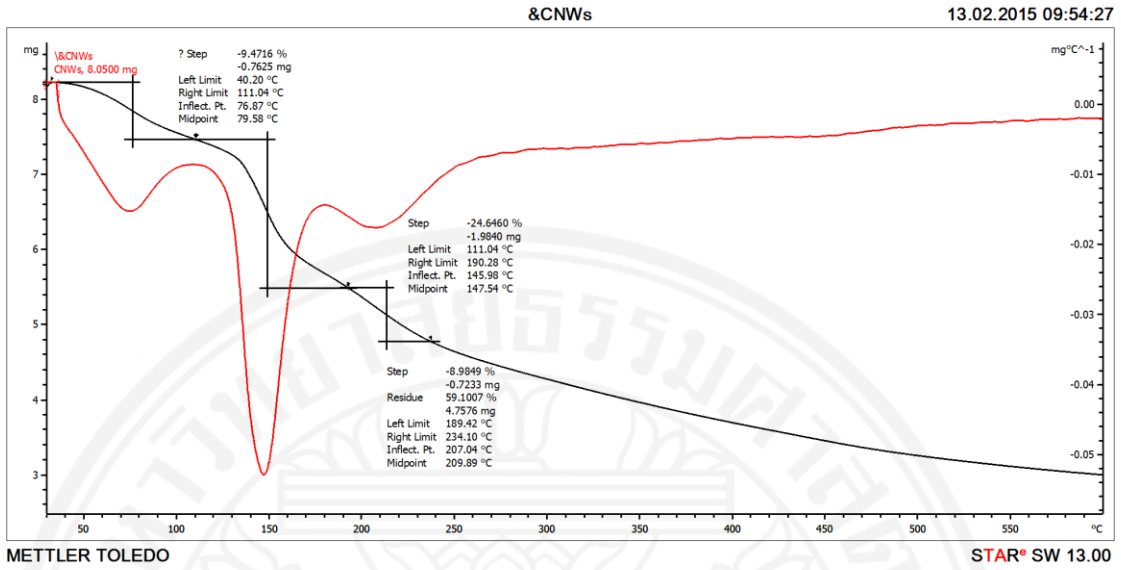**Figure F-12** X-ray diffractogram of 0.5CNC after mechanical testing
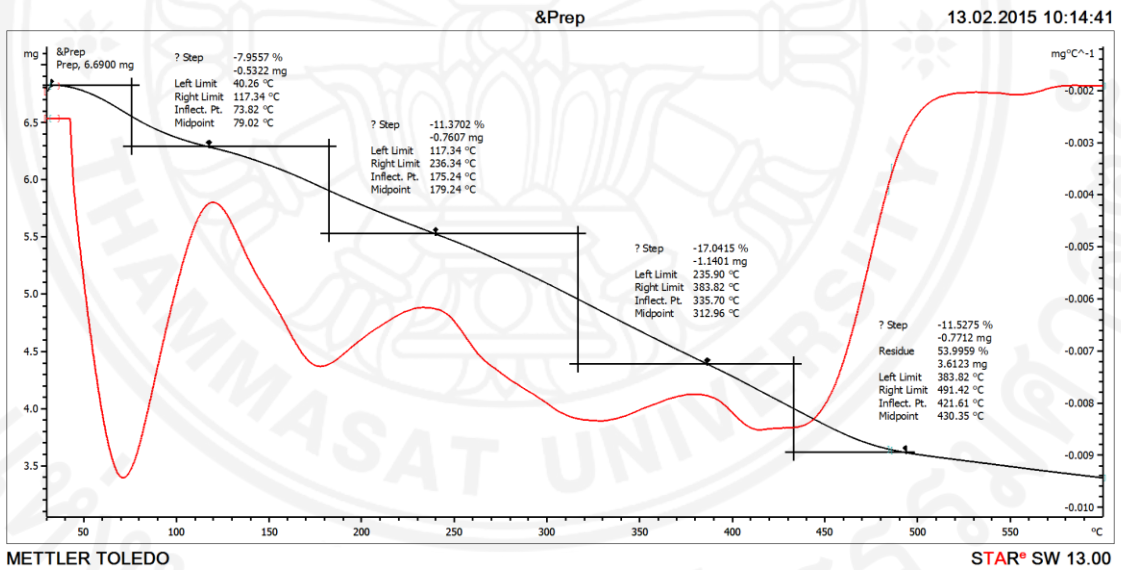
Appendix G

DSC and TGA curves
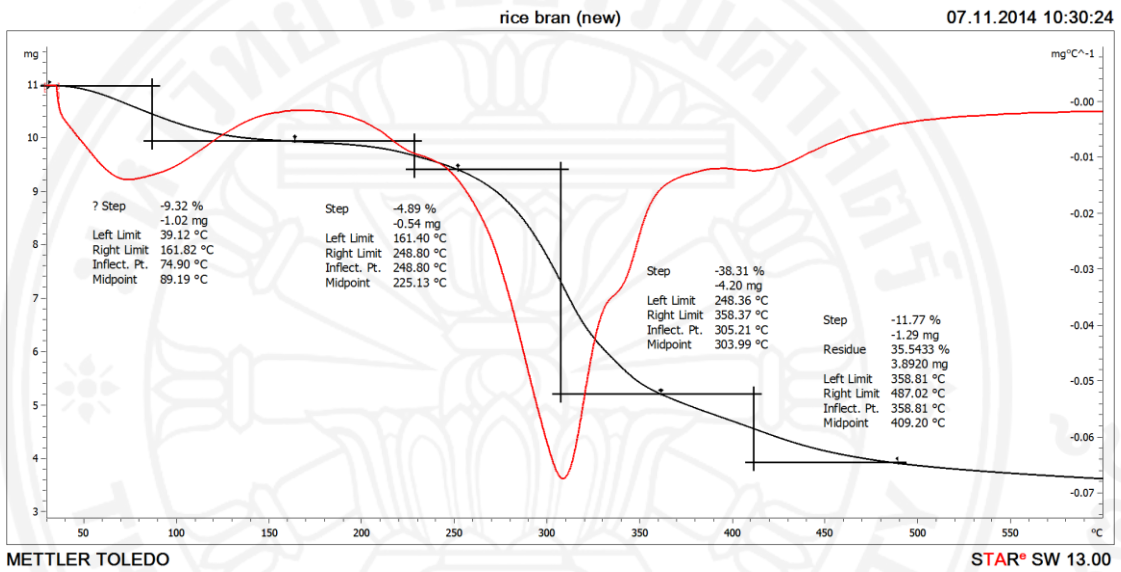
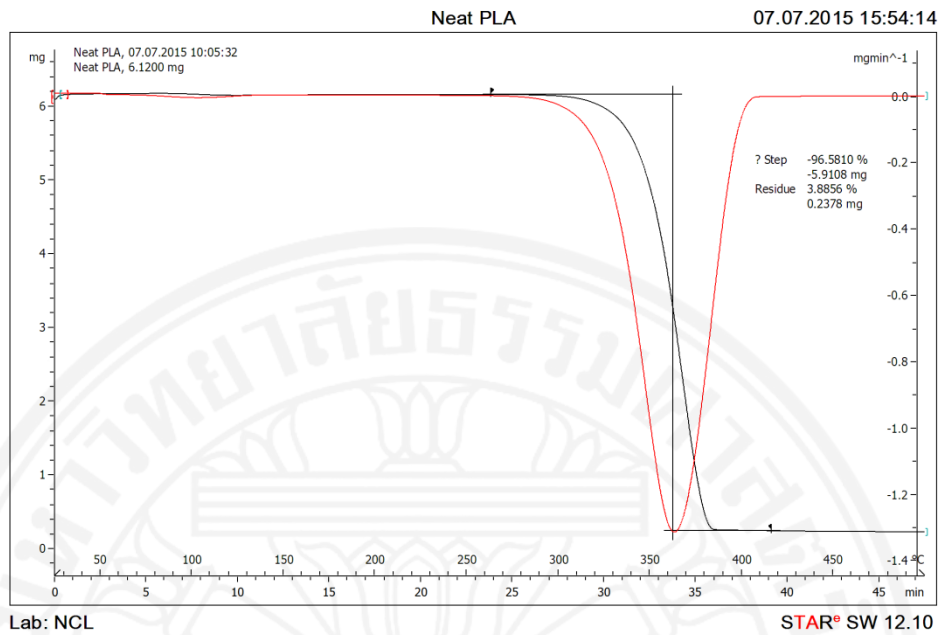**Figure G-1** TGA curve of rice bran waste (RBW)

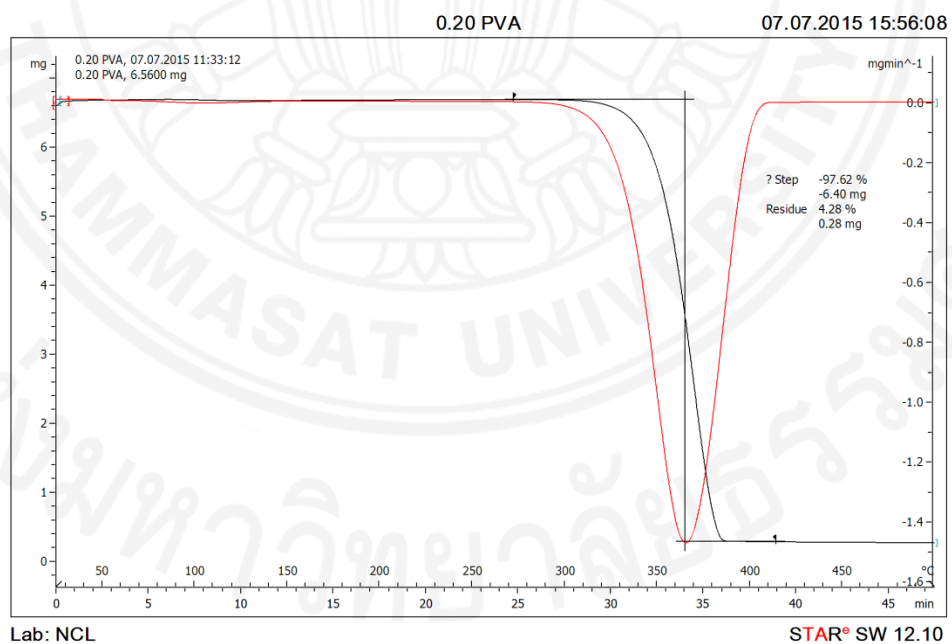**Figure G-2** TGA curve of rice bran cellulose (RBC)

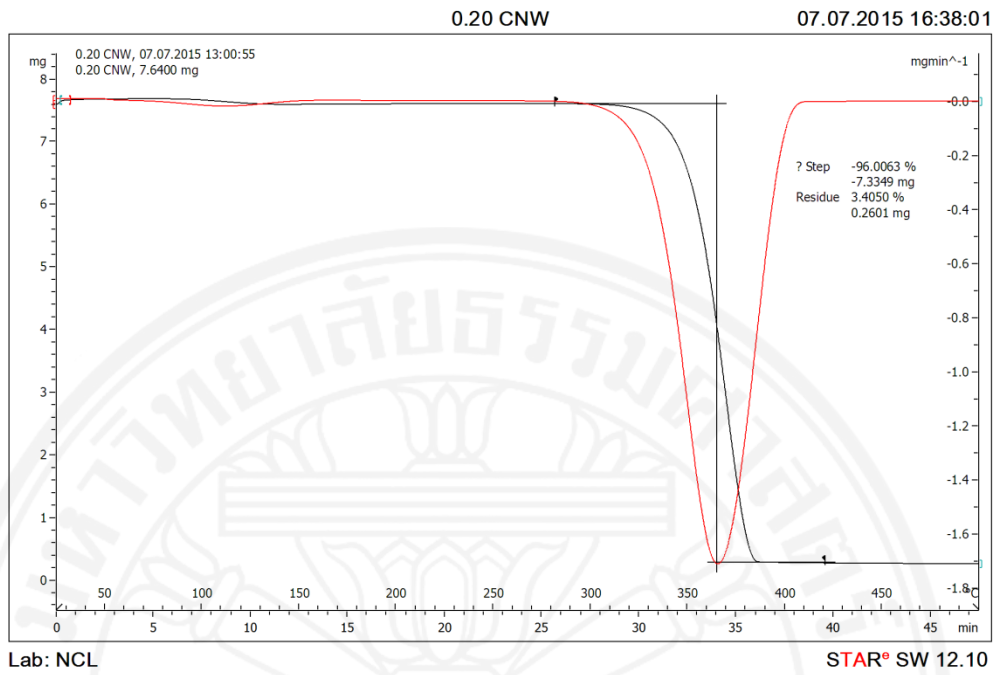**Figure G-3** TGA curve of cellulose nanocrystals (CNC)

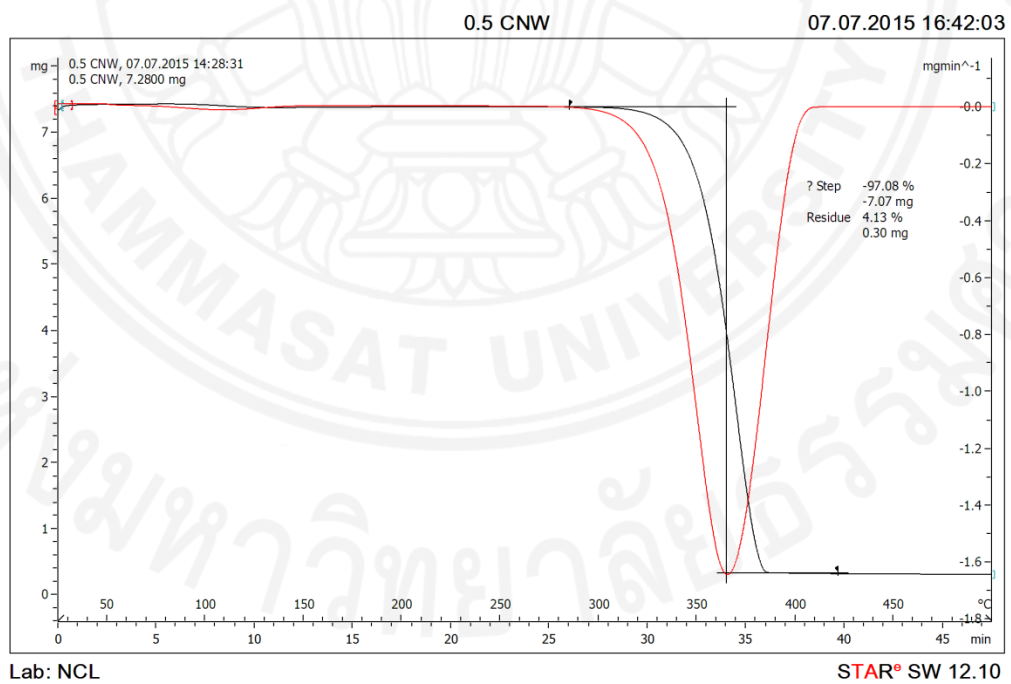**Figure G-4** TGA curve of cellulose nanocrystals precipitate (PREP)

Figure G-5 TGA curve of neat PLA film

Figure G-6 TGA curve of 0.2CNC-PVA film

Figure G-7 TGA curve of 0.2CNC film

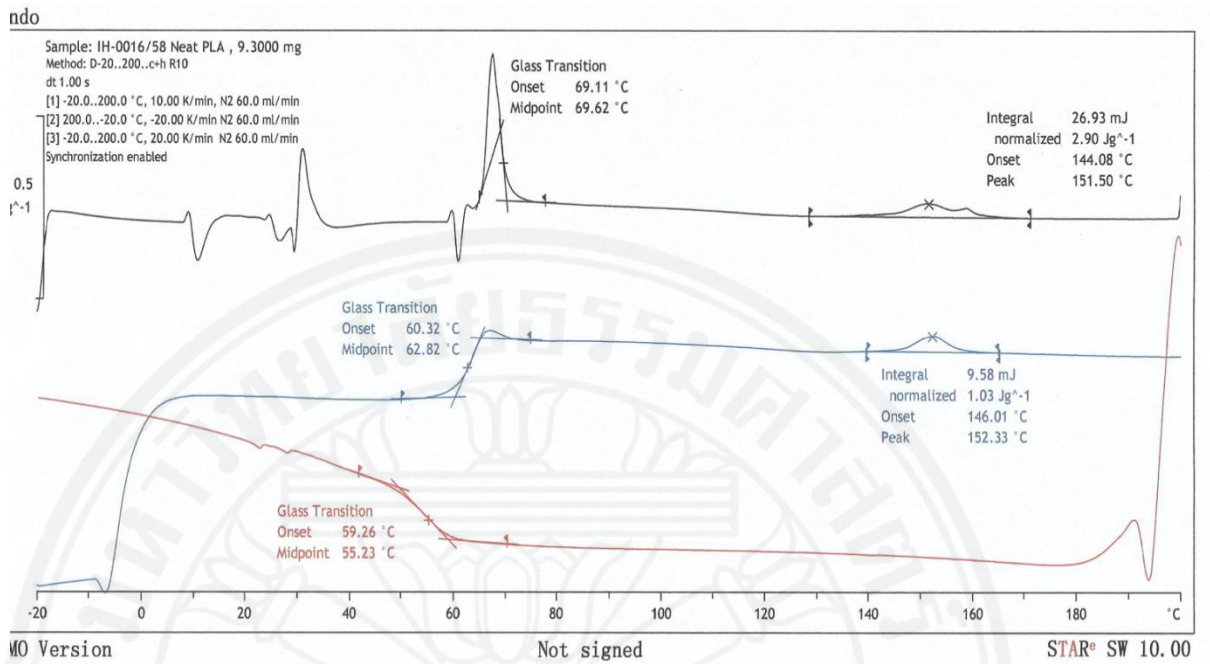**Figure G-8** TGA curve of 0.5CNC film
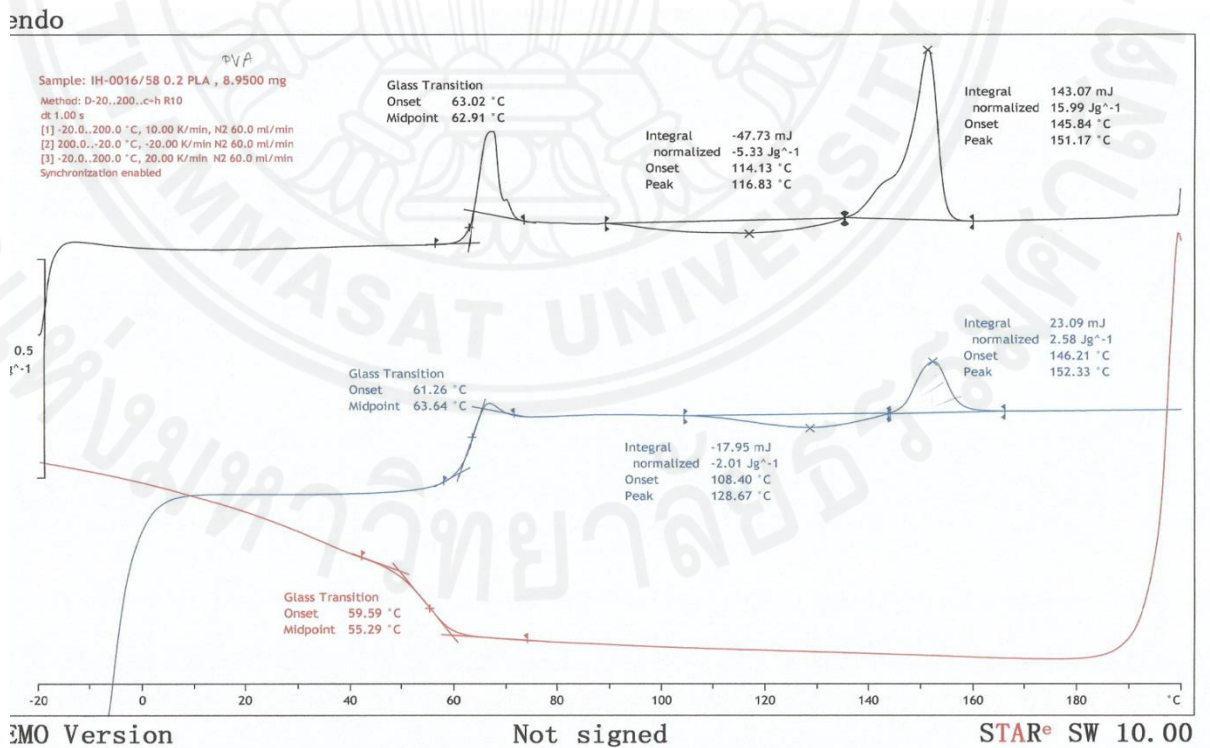
Figure G-9 DSC curve of neat PLA film

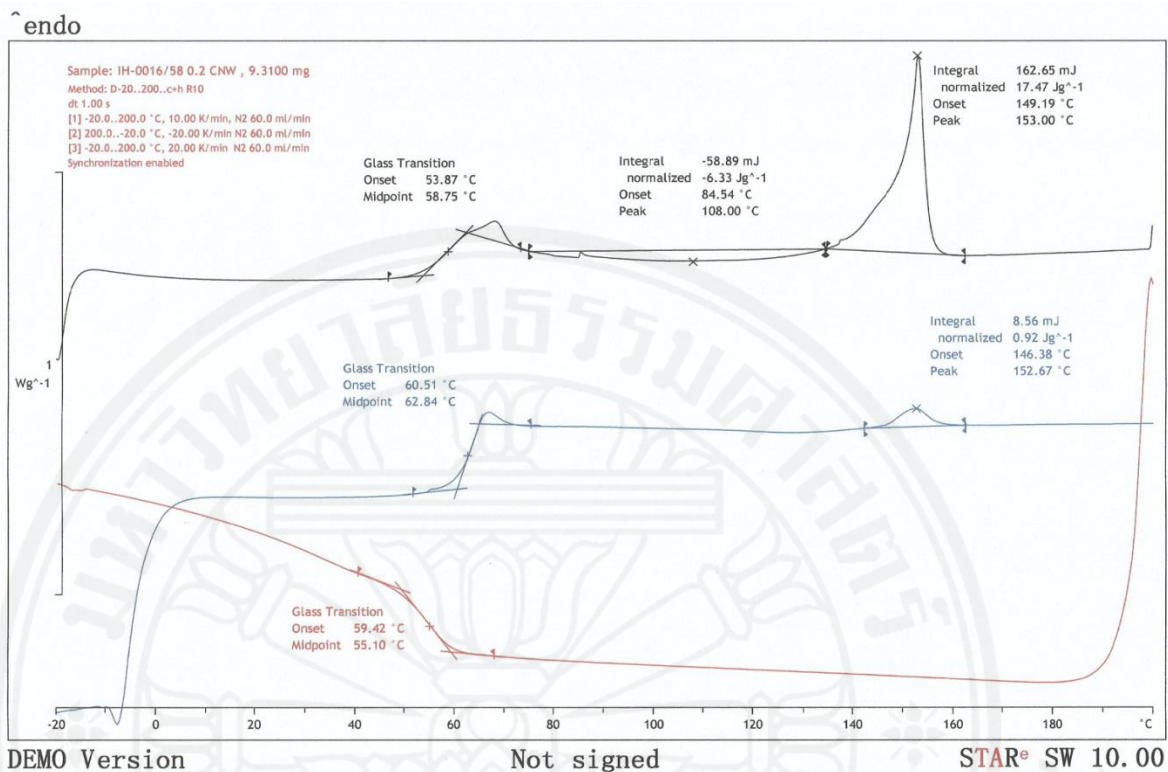**Figure G-10** DSC curve of 0.2CNC-PVA film
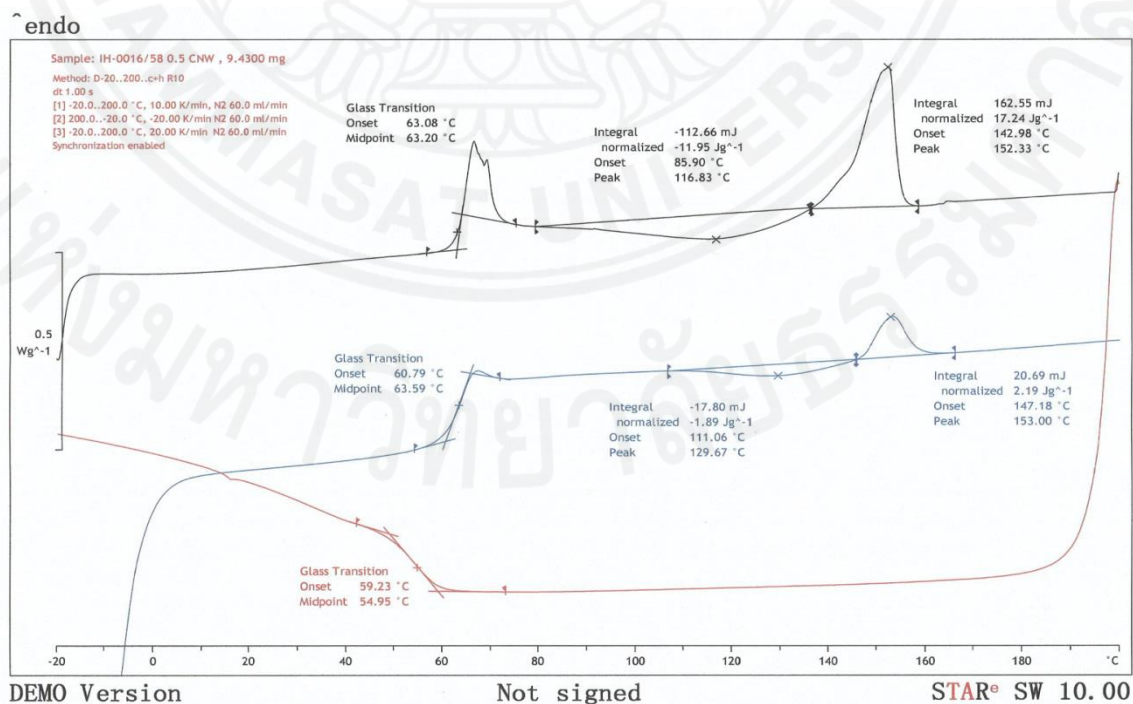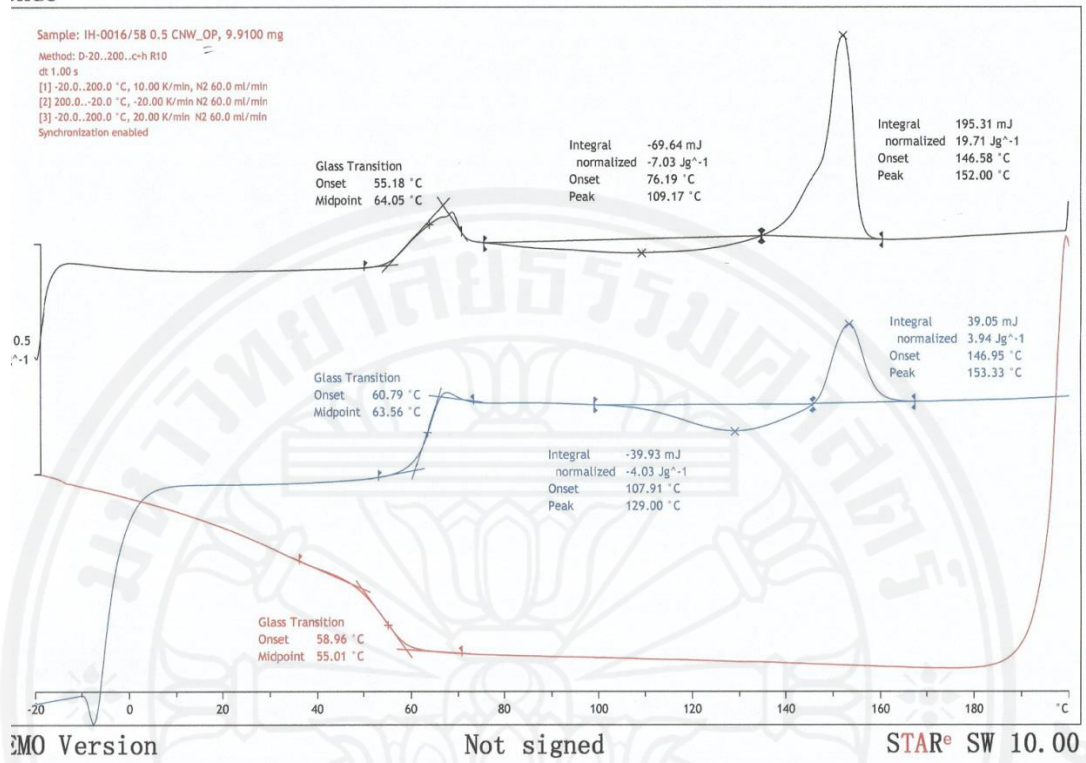
Figure G-11 DSC curve of 0.2CNC film

Figure G-12 DSC curve of 0.5CNC film

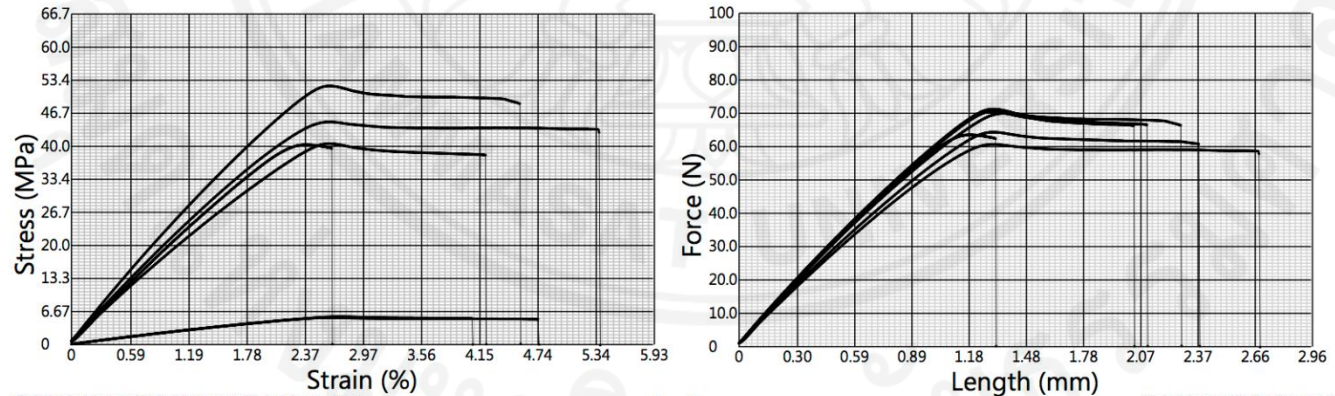**Figure G-13** DSC curve of 0.5CNC_OP (opaque zone of 0.5CNC film)

Appendix H

Mechanical properties

NO	Width mm	Thickness mm	Area mm²	Gage Length mm	Yield Stress MPa	Yield Strain %	E Modulus MPa	Tensile Strength MPa	Elongation %	Secant Modulus MPa	Break Energy MJ/m³
1	15.00	0.09	1.35	50.00	N/F	N/F	2077.472	44.938	5.376	2119.912	1884336.245
2	15.00	0.09	1.37	50.00	N/F	N/F	2349.109	52.161	4.571	2385.008	1749020.973
3	15.00	0.11	1.58	50.00	N/F	N/F	2053.445	40.317	2.654	2010.790	652544.894
4	15.00	0.83	12.50	50.00	N/F	N/F	249.936	5.597	4.084	252.897	160704.845
5	15.00	0.79	11.90	50.00	N/F	N/F	249.806	5.406	4.758	251.144	192245.439
6	15.00	0.12	1.74	50.00	N/F	N/F	1847.098	40.555	4.222	1864.085	1224275.554
Average					N/A	N/A	1471.144	31.496	4.277	1480.639	977187.992
SD					N/A	N/A	959.363	20.587	0.916	966.815	757346.558

ASTM D882-10: Tensile Properties of Thin Plastic Sheeting (Ver. 1), [SIT - Tensile Properties of Thin P]
v10.1.0.0 - 324777GB

- Page 1 -

SIT - Tensile Properties of Thin Plastic Sheeting (rev. 20)
H5K : 1000N. Printed: 6/5/2015 11:18 AM

Figure H-1 Mechanical results and graphs of neat PLA film

NO	Width mm	Thickness mm	Area mm²	Gage Length mm	Yield Stress MPa	Yield Strain %	E Modulus MPa	Tensile Strength MPa	Elongation %	Secant Modulus MPa	Break Energy MJ/m³
1	15.00	0.09	1.29	50.00	N/F	N/F	2069.071	43.152	5.038	2076.759	1592502.334
2	15.00	0.05	0.68	50.00	N/F	N/F	2379.035	41.728	4.956	2419.946	1634873.163
3	15.00	0.08	1.22	50.00	N/F	N/F	2481.629	49.547	5.484	2432.930	2148149.102
4	15.00	0.07	1.02	50.00	N/F	N/F	2422.914	44.935	7.094	2421.682	2559842.677
Average					N/A	N/A	2338.162	44.841	5.643	2337.829	1983841.819
SD					N/A	N/A	184.252	3.401	0.995	174.142	459601.127

ASTM D882-10: Tensile Properties of Thin Plastic Sheeting (Ver. 1), (SIIT - Tensile Properties of Thin P]
v10.1.0.0 - 324777GB

- Page 1 -

SIIT - Tensile Properties of Thin Plastic Sheeting (rev. 20)
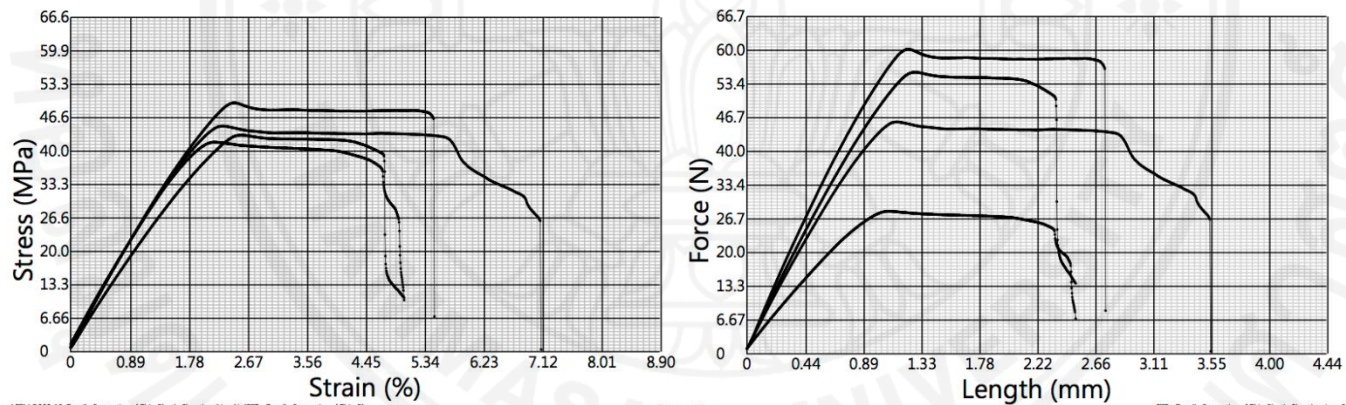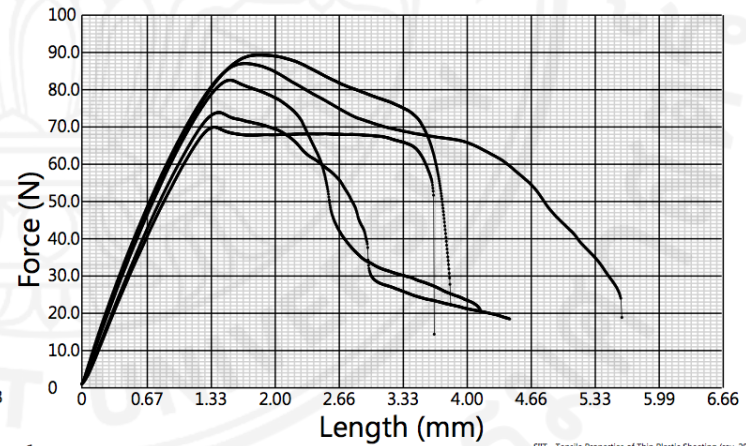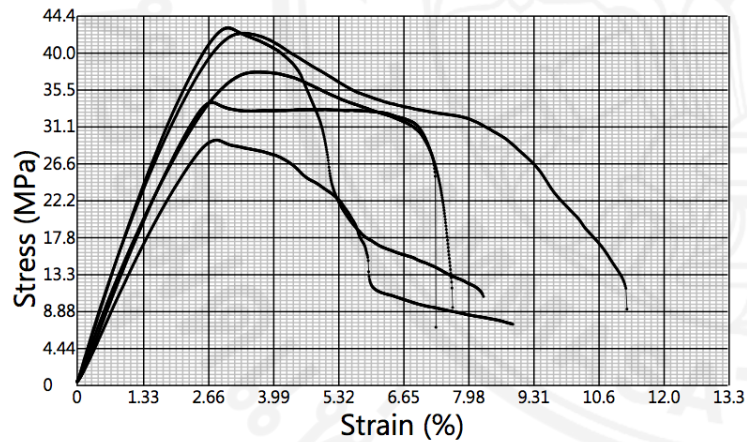H5K : 1000N. Printed: 6/5/2015 12:02 PM

Figure H-2 Mechanical results and graphs of 0.2CNC-PVA film

	Product Name:	0.2 CNW			Speed: 1.00 mm/min					
	Product Number:	3								
	Operator:	Aey								
	Date:	05/06/2015								

NO	Width mm	Thickness mm	Area mm²	Gage Length mm	Yield Stress MPa	Yield Strain %	E Modulus MPa	Tensile Strength MPa	Elongation %	Secant Modulus MPa	Break Energy MJ/m³
1	15.00	0.16	2.37	50.00	N/F	N/F	1601.091	37.665	7.526	1534.568	2162367.335
2	15.00	0.13	1.92	50.00	N/F	N/F	1839.111	42.986	8.308	1835.498	2088035.807
3	15.00	0.14	2.06	50.00	N/F	N/F	1851.787	42.336	11.220	1820.451	3333121.864
4	15.00	0.14	2.06	50.00	N/F	N/F	1561.824	34.031	7.292	1476.940	2011005.507
5	15.00	0.17	2.51	50.00	N/F	N/F	1300.344	29.488	8.908	1268.625	1543755.060
Average					N/A	N/A	1630.831	37.301	8.651	1587.216	2227657.115
SD					N/A	N/A	227.525	5.691	1.573	241.079	663413.355

ASTM D882-10: Tensile Properties of Thin Plastic Sheeting (Ver. 1), [SIIT - Tensile Properties of Thin P]
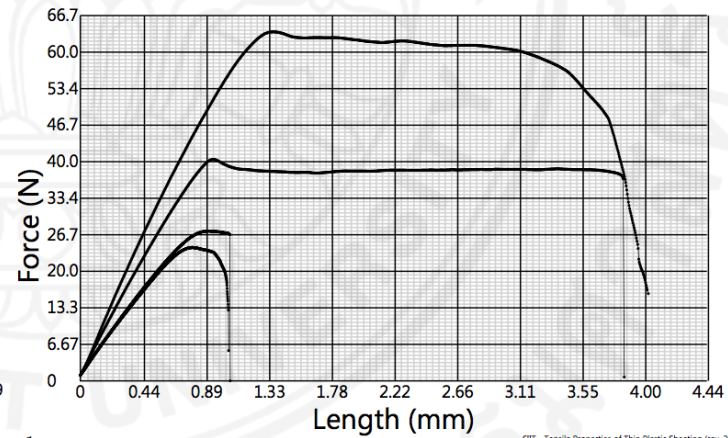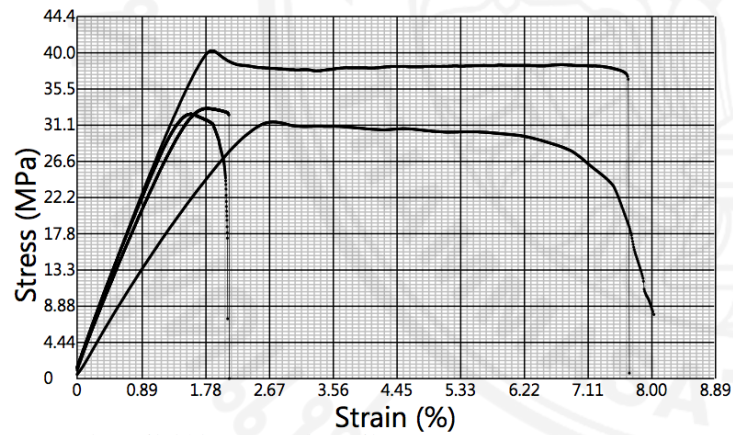v10.1.0.0 - 324777GB

- Page 1 -

SIIT - Tensile Properties of Thin Plastic Sheeting (rev. 20)
H5K : 1000N. Printed: 6/5/2015 12:47 PM

Figure H-3 Mechanical results and graphs of 0.2CNC film

NO	Width mm	Thickness mm	Area mm²	Gage Length mm	Yield Stress MPa	Yield Strain %	E Modulus MPa	Tensile Strength MPa	Elongation %	Secant Modulus MPa	Break Energy MJ/m³
1	15.00	0.14	2.03	50.00	N/F	N/F	1501.975	31.473	7.898	1465.241	1993089.500
2	15.00	0.06	0.83	50.00	N/F	N/F	2249.239	33.131	2.120	2254.125	461316.103
3	15.00	0.07	1.01	50.00	40.199	1.867	2430.443	40.199	7.692	2467.737	2650231.644
4	15.00	0.05	0.75	50.00	N/F	N/F	2423.914	32.444	2.072	2415.944	454322.025
Average					40.199	1.867	2151.393	34.312	4.945	2150.762	1389739.818
SD					N/A	N/A	441.004	3.983	3.292	465.982	1109030.737

ASTM D882-10: Tensile Properties of Thin Plastic Sheeting (Ver. 1), [SIIT - Tensile Properties of Thin P]
v10.1.0.0 - 324777GB

- Page 1 -

SIIT - Tensile Properties of Thin Plastic Sheeting (rev. 20)
H5K : 1000N. Printed: 6/5/2015 1:25 PM

Figure H-4 Mechanical results and graphs of 0.5CNC film